Draft version May 14, 2014
Preprint typeset using LaTeX style emulateapj v. 5/2/11

arXiv:1405.3268v1 [astro-ph.GA] 13 May 2014

MULTILAYER FORMATION AND EVAPORATION OF DEUTERATED ICES IN PRESTELLAR AND PROTOSTELLAR CORES

Vianney Taquet[1,2], Steven B. Charnley[2], and Olli Sipilä[3]

(Dated: Received - ; accepted -)
Draft version May 14, 2014

ABSTRACT

Extremely large deuteration of several molecules has been observed towards prestellar cores and low-mass protostars for a decade. New observations performed towards low-mass protostars suggest that water presents a lower deuteration in the warm inner gas than in the cold external envelope. We coupled a gas-grain astrochemical model with a one-dimension model of collapsing core to properly follow the formation and the deuteration of interstellar ices as well as their subsequent evaporation in the low-mass protostellar envelopes with the aim of interpreting the spatial and temporal evolutions of their deuteration. The astrochemical model follows the formation and the evaporation of ices with a multilayer approach and also includes a state-of-the-art deuterated chemical network by taking the spin states of H_2 and light ions into account. Because of their slow formation, interstellar ices are chemically heterogeneous and show an increase of their deuterium fractionation towards the surface. The differentiation of the deuteration in ices induces an evolution of the deuteration within protostellar envelopes. The warm inner region is poorly deuterated because it includes the whole molecular content of ices while the deuteration predicted in the cold external envelope scales with the highly deuterated surface of ices. We are able to reproduce the observed evolution of water deuteration within protostellar envelopes but we are still unable to predict the super-high deuteration observed for formaldehyde and methanol. Finally, the extension of this study to the deuteration of complex organics (COMs), important for the prebiotic chemistry, shows a good agreement with the observations, suggesting that we can use the deuteration to retrace their mechanisms and their moments of formation.

Subject headings: astrochemistry — ISM: abundances — ISM: molecules — stars: formation

1. INTRODUCTION

The early stages of low-mass star formation are characterized by extremely enhanced molecular deuteration observed for various gaseous species. In spite of the low cosmic elemental reservoir of deuterium (1.5×10^{-5}, Linsky 2003), the deuterium fractionation[4] of simply and doubly deuterated species can reach $\sim$ 50 % and $\sim$ 15 %, respectively in low-mass prestellar cores and Class 0 protostars (Parise et al. 2006; Bergman et al. 2011) while triply deuterated isotopologues have also been detected (Parise et al. 2004; Roueff et al. 2005).

The deuterium chemistry in the gas phase is believed to be triggered by the deuterium exchange between HD and H_3^+, as the deuterium reservoir is likely initially located in HD, via the reaction

$$H_3^+ + HD \rightarrow H_2D^+ + H_2 + 232 \text{ K}. \quad (1)$$

which is in competition with the reaction between H_3^+ and CO. In dense and cold prestellar cores, the CO freeze-out at the surface of interstellar grains increases the reactivity of reaction (1) as well as its deuterated analogues through the decrease of the destruction of H_3^+ via the reaction between H_3^+ and CO. For high densities and high CO depletions, the gas phase D/H abundance ratio of deuterated species can easily reach 100 % (Roberts et al. 2003). Since reaction (1) is exothermic, its backward process cannot occur in the cold conditions ($T < 20$ K) found in prestellar cores if only the para spin state of H_2 is considered. However, due to its higher internal energy, the ortho spin state allows the reaction between H_2 and H_2D^+ to occur, even at low temperatures. Therefore, the ortho/para ratio of H_2 opr(H_2) strongly influences the deuteration of gaseous species in prestellar cores (Flower et al. 2006).

Millimetric observations performed towards Class 0 protostars have shown that various molecules, mostly formed at the surface of interstellar grains in molecular clouds and evaporated in the warm inner regions of protostellar envelopes at $T > 100$ K (the so-called hot corinos), show different deuterations. For example, in the low-mass protostar prototype IRAS 16293-2422 (hereafter I16293), formaldehyde and methanol show higher deuterations (with D/H ratios of 15 and 40 %, respectively, see Loinard et al. 2001; Parise et al. 2002, 2004) than ammonia and water ($\sim$ 10 and 3 %, respectively, see van Dishoeck et al. 1995; Coutens et al. 2012). The deuterium fractionation can be used as a chemical tool to retrace the history of interstellar ices and gas-grain astrochemical models have been developed to interpret the observations of low-mass protostars (Cazaux et al. 2011; Taquet et al. 2012b, 2013a). The lower deuterium fractionation of water with respect to that of formalde-

[1] NASA Postdoctoral Program Fellow
[2] Astrochemistry Laboratory and The Goddard Center for Astrobiology, Mailstop 691, NASA Goddard Space Flight Center, 8800 Greenbelt Road, Greenbelt, MD 20770, USA
[3] Department of Physics, PO Box 64, 00014 University of Helsinki, Finland

[4] In the following of this manuscript, the deuterium fractionation, also referred as the D/H abundance ratio, of a deuterated species XD stands for the abundance ratio between this deuterated species and its main isotopologue XH: D/H(XD) = [XD]/[XH].

hyde and methanol is likely due to a different epoch of formation. Water would be mainly produced for typical molecular cloud conditions (low density and warm temperature) while most of formaldehyde and methanol would be formed afterwards, during the colder and denser prestellar phase. A low opr(H_2), lower than 10^{-3}, is also required to reproduce the observed deuterations (Taquet et al. 2013a).

Because of its high sensitivity to the variation of physical and chemical parameters, the deuterium fractionation can also be used to probe the chemical evolution through the formation of low-mass stars like the Sun. The comparison of the molecular content observed in prestellar cores and low-mass protostars with that found in Solar System comets and meteorites shows that the deuterium fractionation of water and organics decreases by several orders of magnitude (from 1 - 100 % to 0.01 - 0.1 %, see Ceccarelli et al. 2014). The decrease of the D/H ratio with the evolutionary stage of star formation can be interpreted by the chemical alteration of the molecular content in protoplanetary disks and in the solar nebula. Molecules observed in protostellar envelopes will be eventually recycled in protoplanetary disks due to the high turbulent mixing and the strong UV and X-ray radiation fields irradiating the disks (Furuya et al. 2013; Albertsson et al. 2014). The difference of deuteration could also come from the different scales probed by the astronomical observations and by the study of solar system bodies. Most of the meteorites and comets studied in our Solar System were initially relatively closed to the Sun (< 50 AU) while most of sub-millimetric astronomical observations of low-mass protostars are sensitive to much larger scales of several hundreds/thousands of AU (see Ceccarelli et al. 2014).

New observations of deuterated water performed with the *Herschel Space Observatory* (Coutens et al. 2013a,b) as well as ground-based interferometers (Persson et al. 2013; Visser et al. 2013; Taquet et al. 2013b; Persson et al. 2014.) towards low-mass protostars have allowed astronomers to probe the deuteration of warm water originating from the inner regions of protostellar envelopes (< 100 AU), and suggest that warm water shows a lower deuteration ([HDO]/[H_2O] $\sim 0.1-1$ %) than the values derived in previous studies with single-dish telescopes (1 - 10 %, Liu et al. 2011; Coutens et al. 2012). Moreover, Coutens et al. (2013a,b) showed that the deuteration of cold water originating from the external envelope would be higher (~ 1 %) than the deuteration of warm inner water. These observations, therefore, suggest an evolution of the deuteration within protostellar envelopes encompassed by the large beam of single-dish telescopes used so far to study the deuteration of most of molecules. Consequently, astrochemical models have to to be coupled with evolutionary models to properly follow the deuteration within prestellar cores and protostellar envelopes. A previous attempt has been made by Aikawa et al. (2012) who followed the evolution of the molecular deuteration from molecular clouds to protostellar envelopes through the coupling of a gas-grain astrochemical model with a one-dimensional radiative hydrodynamic model. These authors showed an evolution of the chemical abundances of icy species and complex organics with the age of the protostar and gave predictions for their deuterium fractionation. However, they used a standard two-phase gas-grain astrochemical model which did not allow them to distinguish the chemical processes between the ice surface and the ice mantle, a crucial aspect for the modelling of deuterated ices (Taquet et al. 2012b), and did not include the effect of the spin states of H_2 on the deuterium chemistry.

The ortho/para ratio of H_2 is believed to evolve in molecular clouds from a high ortho/para ratio, induced by its formation at the surface of interstellar grains as recently observed in laboratory experiments (Watanabe et al. 2010) to its low Boltzmann value ($< 10^{-4}$), with a timescale comparable to the lifetime of molecular clouds ($\sim 10^7$ yr, see Flower et al. 2006). The slow decrease of the opr(H_2) is supported by the non-detection of DCO^+ towards interstellar clouds outside dense cores which has been attributed by Pagani et al. (2011) to an opr(H_2) higher to 0.1. Since interstellar ices start to form in translucent regions of molecular clouds, when the visual extinction exceeds ~ 3 mag (Whittet et al. 1988), a part of these interstellar ices would likely form when the opr(H_2) is still high.

In this work, we aim at self-consistently studying the deuterium chemistry from molecular clouds to protostellar envelopes. For this purpose, we coupled our astrochemical model GRAINOBLE with a simple, but accurate, one-dimensional evolutionary model of core collapse and we included the spin states of H_2 and light ions that are of crucial importance for the deuterium chemistry. We will focus our study on the formation, the deuteration and the evaporation of interstellar ices and complex organics, which are believed to be relevant for the prebiotic chemistry found in the Solar System (see Pizzarello & Huang 2005; Mumma & Charnley 2011). The physical code and the astrochemical model are described in section 2. In section 3, we present the evolution of the molecular deuteration by focusing our study on the main ice components and on complex organics formed at the surface of grains. We then discuss the implications of our work in section 4 and present our conclusions in section 5.

2. MODEL

2.1. *Dynamical Model*

This section describes the physical model used in this work to follow the formation of a prestellar core and its collapse, giving birth to a central protostar surrounded by a protostellar envelope. The physical evolution can be divided into three steps: 1) the static formation of the dense core for $t < 0$, where $t = 0$ is defined as the beginning of the core contraction; 2) the collapse of the dense core for $0 < t < t_{\rm FF}$, where $t_{\rm FF}$ is the free-fall timescale of the core; 3) the birth of the protostar and the collapse of the protostellar envelope for $t_{\rm FF} < t < t_{\rm FF}+t_{\rm C0}$, where $t_{\rm C0}$ is the timescale of the Class 0 stage, defined as the moment when the mass of the central protostar reaches half of the total (protostar+envelope) mass.

We considered 182 shells of gas and dust initially spaced between $1 \leq r \leq 3\times10^4$ AU so they are spaced at logarithmic intervals for specific times during the Class 0 stage. Because the core is evolving dynamically, the position of each shell evolves with time, so it is necessary to solve the chemistry in a frame of reference comoving with the gas in the Lagrangian coordinates.

2.1.1. *Static formation of the core*

We followed the formation of the dense core by assuming a static contraction, starting from a homogeneous translucent sphere of a density $n_{\rm H,ini}$ embedded in surroundings by a visual extinction $A_{V,\rm ext}$. During its static contraction, the core keeps a Plummer-like density profile obtained from this equation

$$n_{\rm H} = \frac{n_{\rm H,0}}{(1+(r/R_{\rm f})^2)^{\eta/2}} \quad (2)$$

where $n_{\rm H,0}$ is the central density, $R_{\rm f}$ is the characteristic radius inside which the density is uniform. Outside $R_{\rm f}$, the density follows a power-law $\rm r^{-\eta}$ when $r >> R_{\rm f}$. $n_{\rm H,0}$ increases with time between $n_{\rm H,ini}$ and the central density of the observed core $n_{\rm H,0,obs}$ (see section 2.1.3) to reach different selected intermediate central densities $n_{\rm H,0}$ in timescales given by their respective free-fall timescale. The choice of the intermediate and final central densities (and of their timescale) is explained in section 2.1.3 and is based on the observational estimates of molecular clouds ages. As R_f is given by the product of the sound speed and the free-fall time of the central density $n_{\rm H,0}$ (Keto & Caselli 2010), $R_{\rm f}$ decreases with $1/\sqrt{n_{\rm H,0}}$.

2.1.2. *Free-fall collapse*

After its static formation, the dense core undergoes a free-fall collapse following the model developed by Whitworth & Ward-Thompson (2001). At $t = 0$, the collapse is triggered artificially, the density and velocity profiles as well as the accretion rate are followed with time from equations (4), (6), and (7) of Whitworth & Ward-Thompson (2001).

Due to the rapid accretion of the inner shells towards the center, a protostar is formed at the center of the envelope once $t = t_{\rm FF}$, with

$$t_{\rm FF} = \sqrt{\frac{3\pi}{32 G n_{\rm H,0,obs} m_p}} \quad (3)$$

where m_p is the proton mass. The gravitational energy of the collapsed mass is released radiatively as the material falls onto the protostar radius $R_\star$. The luminosity of the protostar is, therefore, given by

$$L_\star = \frac{G M_\star \dot{M}_{acc}}{R_\star} \quad (4)$$

where $M_\star$ is the mass of the protostar, and $\dot{M}_{acc}$ is the accretion rate. $\dot{M}_{acc}$ and $M_\star$ are directly given the dynamical model and we derived $R_\star$ from the work by Hosokawa & Omukai (2009) who computed the evolution of the star radius as function of the stellar mass, for different constant accretion rates. Since the accretion rate computed by our code evolves with time, we extrapolated their Fig. 14 by computing the averaged accretion rate at each timestep relative to the beginning of the protostar formation in order to derive an estimate of $R_\star$ for each timestep.

2.1.3. *Physical parameters*

The density profile reached at the end of the static formation phase aims at modelling the starless core L1498. L1498 is thought to have a central density $n_{\rm H,0,obs} = 2 \times 10^5$ cm^{-3} and tends to be extended with a radius $R_{\rm f} = 1 \times 10^4$ AU and presents a steep slope ($\eta = 4$) (Tafalla et al. 2002).

The timescale for the static formation needed to reach the observed profile of the core is based on the timescale estimates derived from observations and models of molecular clouds. The lifetime of molecular clouds is still controversial as two main contradictory theories have been developed. The first one is a quasi-static theory in which clouds are closed to equilibrium, giving long timescales for the evolution of molecular clouds of ~ 10 Myr (Mouschovias et al. 2006). A more recent view of cloud evolution has been proposed, which is based on the importance of supersonic turbulent flows leading to a lack of equilibrium and giving, therefore, shorter timescales of 3-5 Myr (Hartmann et al. 2001). Chemistry can be used as a tracer for the age of molecular clouds. From the non-detection of DCO^+ in dark clouds, Pagani et al. (2011) estimated an upper limit for the clouds age of 6 Myr. Consequently, we can reasonably assess that molecular clouds have a total lifetime of a few Myr. We then derived the total timescale of static formation based on the molecular cloud lifetime estimate and on the free-fall timescale of seven different Plummer-like cores with selected central densities between $n_{\rm H,ini}$ and $n_{\rm H,0,obs}$ (see also Lee et al. 2004a, for a similar method of static formation). Table 1 summarizes the physical properties of the core and compares the different timescales $t_{\rm MC}$ spent in the molecular cloud phase (i.e, when the central density is lower than 5×10^4 yr). Model A-F is a model with a standard static formation while model A-S is a model with a two times longer static formation timescale.

2.2. *Radiative transfer*

We used the radiative transfer code DUSTY (Ivezic & Elitzur 1997) to compute the dust temperature profile of the prestellar and protostellar cores at each timestep. We assumed $T_{\rm g} = T_{\rm d}$, a reasonable assumption for protostellar envelopes (see for instance Maret et al. 2004) and for the central region of dark cores but not necessarily true at the outer edges of dark cores where the gas and dust are thermally decoupled due to the lower density (see Galli et al. 2002; Sipilä 2012). We verified that this assumption is not important for the chemical abundance and deuteration of ices by running two simulations for the streamline at $r = 2 \times 10^4$ AU with two gas phase temperatures: $T_g = T_d = 16$ K (the temperature assumed in the reference model) and $T_g = 10$ K (corresponding to the kinetic temperature derived by Tafalla et al. (2004) at the edge of L1498). The largest differences for the deuteration and the chemical composition of ices are found to be about 30 %. The opacities of dust grains are taken from column 5 in Table 5 of Ossenkopf & Henning (1994) corresponding to grains showing a MRN size distribution covered by thin ice mantles at $n_{\rm H} = 10^6$ cm^{-3}. This data has been successfully used in many works, such as those by van der Tak et al. (2000) and Evans et al. (2001) to model the emission of prestellar and protostellar envelopes.

The thermal structure of the prestellar core is derived from a slab geometry in which the core is irradiated by the Interstellar Radiation Field (ISRF) with a spectrum taken from Evans et al. (2001). We fixed the temper-

TABLE 1
PHYSICAL MODELS AND THEIR PARAMETERS CONSIDERED IN THIS WORK (SEE TEXT FOR A DESCRIPTION OF THE TIMESCALES).

Name	$n_{\rm H,0,obs}$ ($\rm cm^{-3}$)	R_f (AU)	η	M ($M_\odot$)	$t_{\rm MC}$ (yr)	$t_{\rm SC}$ (yr)	$t_{\rm CC}$ (yr)	$t_{\rm C0}$ (yr)
A-F	2×10^5	1.1×10^4	4	5.0	1.7×10^6	2.3×10^5	9.8×10^4	1.0×10^5
A-S	2×10^5	1.1×10^4	4	5.0	3.4×10^6	4.6×10^5	9.8×10^4	1.0×10^5
Observations					$3-6\times10^6$	$2-7\times10^5$	$2-16\times10^4$	$0.4-1.6\times10^5$

NOTE. — $t_{\rm MC}$: lifetime of molecular clouds. $t_{\rm SC}$: lifetime of static cores. $t_{\rm CC}$: lifetime of contracting cores. $t_{\rm C0}$: lifetime of Class 0 protostars.

ature at the edge of the cores to 17 K, following the values derived by Ward-Thompson et al. (2002) towards L1498 at 3×10^4 AU ($\sim 3-4\ '$). Once the protostar has formed at the center of the envelope, the temperature profile is computed with the sphere geometry structure. The effective temperature of the protostar and the grain temperature at $r_{\rm min}=1$ AU, derived from the protostar luminosity, are given as input parameters to the DUSTY code.

2.3. *Astrochemical model*

2.3.1. *Description of the model*

To follow the interstellar gas-grain chemistry, we used our astrochemical model GRAINOBLE presented in previous studies (Taquet et al. 2012a,b, 2013a). GRAINOBLE couples the gas-phase and grain-surface chemistry with the rate equations approach introduced by Hasegawa et al. (1992). The grain surface chemistry processes are the following:

i) The accretion of gas phase species onto the surface of spherical grains with a constant grain radius $r_d=0.1$ μm.
ii) The diffusion of adsorbed species via thermal hopping.
iii) The reaction between two particles once they meet in the same site via the Langmuir-Hinshelwood mechanism. The reaction rate is given by the product of the number of times that the two reactants meet each other and the transmission probability P_r of reaction.
iv) The desorption of adsorbed species into the gas phase, via several processes:
- thermal desorption, which exponentially depends on the binding energy of each species E_b relative to the substrate (see Table 2 for a list of binding energies for selected species).
- cosmic-ray induced heating of grains following Hasegawa & Herbst (1993a) and adapted for the binding energies considered in this work.
- chemical desorption caused by the energy release of exothermic reactions. Following Garrod et al. (2007), we assumed a value of 0.012 for the factor a (the ratio of the surface-molecule bond frequency to the frequency at which energy is lost to the grain surface) for all surface reactions as it seems to be the most consistent value given by molecular dynamics simulations (Kroes & Andersson 2005).
- UV photodissociation and photodesorption. Photodissociation and photodesorption rates of hydrogenated species are derived from molecular dynamics simulations (Andersson et al. 2008) while photodesorption rates of CO, N_2, O_2 are taken from the experimental studies by Fayolle et al. (2011, 2013).

In this work, we adopted the multilayer approach developed by Hasegawa & Herbst (1993b) (see

TABLE 2
SELECTED SURFACE SPECIES AND THEIR BINDING ENERGIES.

Species	$E_{b,\rm bare}$ (K)	$E_{b,\rm wat}$ (K)	$E_{b,\rm pure}$ (K)	Ref.
H	660	500	45	1, 2, 3
C	800	800	800	4
O	800	800	800	4
N	800	800	800	4
S	1100	1100	1100	4
H_2	640	500	45	1, 2, 3
O_2	895	915	915	5, 6
N_2	790	790	790	7
CO	830	1150	855	5, 8, 6
CO_2	2270	2690	2270	5, 9
H_2O	1870	5775	5775	10, 11
NH_3	5535	5535	3080	8, 12
CH_4	1090	1090	1090	13
HCN	2100	2100	2100	14
H_2CO	3260	3260	3765	15
CH_3OH	5530	5530	4230	8, 12
C_2H_2	2600	2600	1830	16
C_2H_4	3600	3600	2060	17
HCOOH	5570	5570	5000	8, 18
CH_3CN	4680	4680	4680	8
$HCOOCH_3$	4630	4630	4000	19, 18
CH_3CHO	3800	3800	3800	18
CH_3OCH_3	4230	4230	3300	19, 18
CH_3CH_2OH	6795	6795	5200	19, 18
NH_2OH	6250	6250	6250	20
CH_3COOH	8155	8155	6300	19, 18
CN	1600	1600	1600	21
CH	870	870	870	22
NH	2380	2380	1560	23
CH_2	945	945	945	24
NH_2	3960	3960	2320	25
CH_3	1017	1017	1017	26
OH	1300	2820	2820	27, 11
HCO	2050	2200	2300	28
CH_3O	3800	3800	4000	29
C_2	1600	1600	1600	30
C_2H	2100	2100	1715	31

NOTE. — [1]: Katz et al. (1999); [2]: Hornekær et al. (2005); [3]: Vidali et al. (1991); [4]: Tielens & Allamandola (1987); [5]: Noble et al. (2012a); [6]: Acharyya et al. (2007); [7]: Bisschop et al. (2006); [8]: Collings et al. (2004); [9]: Sandford & Allamandola (1990); [10]: Avgul & Kiselev (1970); [11]: Fraser et al. (2001); [12]: Sandford & Allamandola (1993); [13]: Herrero et al. (2010); [14]: E_b(C)+E_b(N)+E_b(H); [15]: Noble et al. (2012b); [16]: $E_b(C_2)+2\times E_b$(H); [17]: $E_b(C_2)+4\times E_b$(H); [18]: Öberg et al. (2009); [19]: Lattelais et al. (2011); [20] Congiu et al. (2012); [21]: E_b(N)+E_b(C); [22]: E_b(C)+($E_b(CH_4)$-E_b(C))/4; [23]: E_b(N)+($E_b(NH_3)$-E_b(N))/3; [24]: E_b(C)+($E_b(CH_4)$-E_b(C))/2; [25]: E_b(N)+$2\times(E_b(NH_3)$-E_b(N))/3; [26]: E_b(C)+$3\times(E_b(CH_4)$-E_b(C))/4; [27]: Cuppen & Herbst (2007); [28]: (E_b(CO)+$E_b(H_2CO)$)/2; [29]: ($E_b(H_2CO)$+$E_b(CH_3OH)$)/2; [30]: $2\times E_b$(C); [31]: $2\times E_b$(C)+E_b(H);

also Charnley & Rodgers 2009; Garrod & Pauly 2011; Garrod 2013; Vasyunin & Herbst 2013, for other models adopting a multilayer approach) to follow the multilayer formation and evaporation of interstellar ices since it allows a better treatment of the ice evaporation than the approach used in Taquet et al. (2012a,b, 2013a). The multilayer approach proposed by Hasegawa & Herbst (1993b) considers three sets of differential equations: one for gas phase species, one for surface species, and one for bulk species. The equations governing chemical abundances on the surface and in the bulk are linked via an additional term, proportional to the rate of growth or evaporation of the grain mantle. Surface species are continuously trapped into the bulk because of the accretion of new particles, unlike the approach by Taquet et al. (2012a) in which the trapping is carried out one layer at a time. Using the chemical network and the reference physical conditions adopted in Taquet et al. (2012a), we verified that the two methods give similar ice chemical compositions. The largest difference is found for methanol which shows a difference of 50 % at $t = 10^6$ yr.

2.3.2. *Gas phase chemical network*

The initial chemical network was taken from the KIDA database and includes 11 elements (H, He, C, N, O, Si, S, Fe, Na, Mg, Cl) and 6250 reactions. It has then been extended to include the spin states of H_2, H_2^+, and H_3^+ and the deuterated isotopologues of hydrogenated species with four or less atoms, with some exceptions (see below).

We added the spin states of H_2, H_2^+, and H_3^+ into the KIDA chemical network following the method summarized by Sipilä et al. (2013) in which the separation of each chemical reaction including H_2, H_2^+, or H_3^+ depends on the type of the reaction. There are about 1150 reactions containing H_2, H_2^+, and H_3^+, the ortho/para separation process results in ∼2150 reactions, increasing the number of reactions from 6250 to 7150 reactions.

The chemical network including the spin states of H_2, H_2^+, H_3^+ was then deuterated with the routine developed by Sipilä et al. (2013) (see also Rodgers & Millar 1996; Aikawa et al. 2012; Albertsson et al. 2013, for other generated deuterated networks). Since we aim at following the deuteration of interstellar ices, we are particularly interested in the evolution of the atomic [D]/[H] abundance ratio in the gas phase. We, therefore, included deuterated forms of species with up to four atoms. All reactions including an hydrogenated species are cloned by assuming same rate coefficients. When the final position of the D atom is ambiguous, giving several sets of possible products, statistical branching ratios have been assumed. 2840 reactions containing species with up to four atoms have been deuterated, resulting in new 7900 reactions added to the network. We also deuterated the reactions involved in the gas phase chemical network of H_2O, NH_3, H_2CO, and CH_3OH and which contain molecules with more than four atoms (see Roberts & Millar 2000, for a schematic picture of the water, ammonia, and formaldehyde networks).

Although we aim at investigating the deuterium fractionation of specific complex organics in the hot corino, we chose not to deuterate their formation and destruction reactions in the gas phase. Following recent state-of-the-art gas-grain astrochemical models, the current scenario is that complex organics are mostly formed at the surface of interstellar grains (Garrod et al. 2008) while gas phase reactions would alter their abundances and deuterations in a timescale higher than 10^4 yr (Charnley et al. 1997; Aikawa et al. 2012). Due to the free-fall collapse model used in this work, molecules formed at the surface of grains stay in the warm gas phase after their evaporation for ∼100 yr before being accreted by the protostar. Gas phase reactions are therefore considered as negligible in the formation and the deuteration of complex organics.

The atomic [D]/[H] abundance ratio and the ortho/para ratio of H_2 are mostly governed by deuterium fractionation reactions involving H^+, H_2, H_2^+, H_3^+, and their deuterated isotopologues (see Flower et al. 2006; Taquet et al. 2013a). Deuterium fractionation reactions of the H_3^+-H_2 system have been introduced in the network with the reaction rate coefficients recently computed by Hugo et al. (2009). Deuteration reactions of the important H_2^+-H_2, H_3^+-H, H^+-H_2, CH_3^+-H_2, and $C_2H_2^+$-H_2 systems and recombinations on electronegative charged grains have also been included following Roberts & Millar (2000); Roberts et al. (2003, 2004); Walmsley et al. (2004) and Pagani et al. (2009). Finally, we considered the chemical network involved in the formation of deuterated water at warm temperatures and including neutral-neutral and radical-neutral reactions, following Thi et al. (2010). We therefore added about 3000 reactions to the deuterated KIDA network, resulting in a gas phase chemical network of 15260 reactions.

2.3.3. *Surface chemical network*

The formation of the main ice species (H_2O, CO_2, H_2CO, CH_3OH, NH_3, CH_4) along with their deuterated isotopologues was followed with the chemical network developed by Taquet et al. (2013a) from laboratory experiments showing the efficient formation of interstellar ice analogs on cold surfaces. The transmission probability of chemical reactions with activation energy barriers included in the water and carbon dioxide networks as well as the key reaction CO+H have been computed with the Eckart model. Transmission probabilities of addition, substitution, and abstraction reactions included in the methanol network have been deduced from the rates experimentally derived by Hidaka et al. (2009).

We also added the surface network introduced by Garrod et al. (2008) to form complex organics. Primary radical-primary radical, primary radical-secondary radical reactions, and reactions between aldehydes and H atoms have been incorporated to our network and extended to include their deuterated counterparts by assuming statistical branching ratios. The transmission probabilities through quantum tunneling of the aldehyde-H reactions have been computed by assuming rectangular energy barriers with a width $a = 1$ Å. In total, the gas-grain chemical network includes about 2700 species and 24500 chemical processes.

For each species i, the effective binding energy $E_b(i)$ relative to the surface was derived from the fractional coverage of i, $P(i)$ and H_2, $P(H_2)$ on the surface layer and from the fraction of bare surface, $P_{\rm bare}$ lying under

the surface layer, following this formula:

$$E_b(i) = (\ 1 - P(\mathrm{H_2}) - P(i) - P_{\rm bare}) \times E_{b,\rm wat}(i) \quad (5)$$
$$+ P(\mathrm{H_2}) \times E_{b,\mathrm{H2}}(i) + P_{\rm bare} \times E_{b,\rm bare}(i) \quad (6)$$
$$+ P(i) \times E_{b,\rm pure}(i)$$

where $E_{b,\rm wat}(i)$, $E_{b,\mathrm{H2}}(i)$, $E_{b,\rm bare}(i)$, and $E_{b,\rm pure}(i)$ are the binding energies of species i relative to amorphous solid water (ASW) ice, H_2 ice, a bare (amorphous carbon or silicate) substrate and a pure ice. To deduce $E_{b,\mathrm{H2}}$ for all species, we applied the scaling factor

$$E_{b,\mathrm{H2}}(i) = E_{b,\mathrm{H2}}(\mathrm{H}) \times \frac{E_{b,\rm wat}(i)}{E_{b,\rm wat}(\mathrm{H})} \quad (7)$$

where $E_{b,\mathrm{H2}}(\mathrm{H})$ is 45 K (Vidali et al. 1991). Table 2 lists the sets of binding energies of selected species for different substrates. In spite of their higher mass, deuterated isotopologues seems to show similar binding energies than their main isotopologue (see Taquet et al. 2013a, for a discussion of the binding energy values). We therefore assumed the same binding energies for all deuterated species and their main isotopologue.

2.3.4. *Input parameters*

The initial elemental abundances in the gas phase considered in this work are listed in Table 3. The elemental abundances of species other than He and HD correspond to the set EA1 from Wakelam et al. (2008). The initial abundances of He and HD are taken from the set EA2 from Wakelam et al. (2008) and from Linsky (2003), respectively.

TABLE 3
Initial elemental abundances in the gas phase with respect to hydrogen nuclei.

Species	Abundance
H_2	0.5
HD	1.6×10^{-5}
He	9.0×10^{-2}
C	7.3×10^{-5}
N	2.1×10^{-5}
O	1.8×10^{-4}
Si	8.0×10^{-9}
S	8.0×10^{-8}
Fe	3.0×10^{-9}
Na	2.0×10^{-9}
Mg	7.0×10^{-9}
Cl	1.0×10^{-9}

The value of the ortho/para ratio of H_2 in molecular clouds is still highly uncertain. The initial value of H_2 opr formed on grain surfaces is most likely 3, as recently confirmed by the experiment by Watanabe et al. (2010) conducted on amorphous solid water. However, proton-exchange reactions in the gas phase would then convert ortho-H_2 to para-H_2, decreasing the opr(H_2) towards the Boltzmann value ($\sim 3 \times 10^{-7}$ at 10 K, see Flower et al. 2006). Pagani et al. (2011) interpreted the non-detection of DCO^+ towards dark cloud envelopes with an opr(H_2) higher than 0.1. However, indirect estimates of H_2 based on the comparison between observations of dark cores or cold protostellar envelopes with chemical models suggest lower values of about $10^{-3} - 10^{-2}$ (Pagani et al. 2009; Dislaire et al. 2012; Le Gal et al. 2013). In this work, the standard value for the initial opr(H_2) is set to 10^{-2}. This value corresponds to an average between the values derived in the early stages (dark cloud envelopes) and the late stages (protostellar envelopes) of molecular evolution. Nevertheless, given the relative uncertainty of this value and its importance in the molecular deuteration process, we also studied the effect of other initial opr(H_2) values (10^{-4} and 3) on the ice deuteration.

We aimed at investigating the influence of some physical parameters on the formation and the deuteration of interstellar ices. Therefore, we assumed several values for the timescale of static formation, initial density, visual extinction and temperature at the edge of the core, listed in Table 4. We also considered an other core, model B, aiming at modelling the well-known core L1544, showing a higher central density $n_{\rm H,0,obs} = 4 \times 10^6$ cm^{-3}, a smaller characteristic radius $R_{\rm f} = 2 \times 10^3$ AU, and a shallower slope $\eta = 2.5$ (Crapsi et al. 2007) than L1498.

As discussed in Taquet et al. (2012a) and Taquet et al. (2013a), the binding energy of light particles E_b and the diffusion to binding energy ratio E_d/E_b show distributions of values depending on the ice composition and morphology. We, therefore, explored several values for these two parameters in a range given by the literature.

We kept fixed the following other parameters:
- distance between two binding sites $d_s = 3.1$ Å;
- cosmic-ray ionization rate $\zeta = 3 \times 10^{-17}$ s^{-1};
- interstellar radiation field (ISRF) $F_{\rm ISRF} = 1 \times 10^8$ photons cm^{-2} s^{-1};
- cosmic ray induced radiation field (CRH2RF) $F_{\rm CRH2RF} = 5 \times 10^4$ photons cm^{-2} s^{-1};
- scaling factor in multiples of the local interstellar field $G_0 = 10$.

TABLE 4
List of free input parameters and their value range explored in this work.

Input parameters	Values
Type of core	**A** - B (see text)
$n_{\rm H,ini}$ (cm^{-3})	$\mathbf{3 \times 10^3}$ -10^4
$A_{\rm V,ext}$ (mag)	1 - **2**
$T_{\rm d,ext}$ (K)	14 - **17** - 20
$t_{\rm BC}$ (yr)	$\mathbf{1 - 2 \times} t_{\rm BC}$
o/p(H_2)$_{\rm ini}$	1×10^{-4} - $\mathbf{1 \times 10^{-2}}$ - 3
E_d/E_b	0.5 - **0.65** - 0.8
E_b(H) (K)	400 - **500** - 600

Note. — Bold values mark the values adopted in the reference model.

3. RESULTS

3.1. *Physical model validation*

Figure 1 presents the physical (density, temperature, velocity) profiles and the accretion rate of the modelled core A-F as a function of time, from the beginning of the translucent phase to the end of the Class 0 stage. $t = 0$ is defined as the beginning of the core collapse, negative times stand for the static formation of the dense core while positive times correspond the dynamical collapse of the core.

For $0 < t < t_{\rm FF}$, the core shows slow internal motions that decrease proportionally with the radius towards the

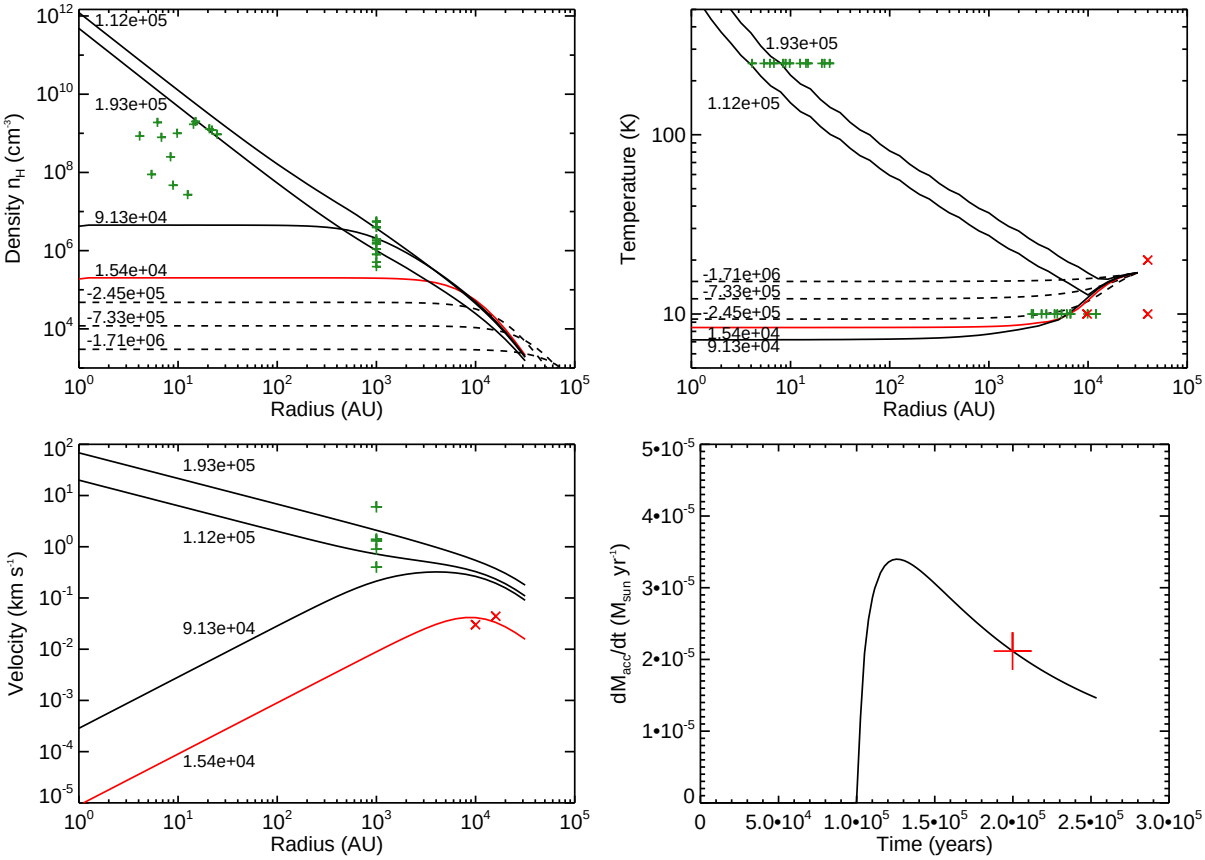

FIG. 1.— Density (top left), temperature (top right), and infall velocity (bottom left) profiles of model A-F plotted for different times and overplotted with observational data of prestellar (red crosses) and protostellar (green plus) cores (see text for more details). Bottom right: Evolution of the accretion rate as a function of time. The red cross represents the end of the Class 0 stage defined as the time when the mass of the protostar reaches half of the total (protostar+envelope) mass.

center. The core keeps its Plummer-like structure, the density profiles are flat in the center at $r < R_f$ and steepen towards the edge. However, with time, the central density slowly increases while R_f decreases. When one free-fall time is reached, all the shells located inside R_f collapse almost simultaneously because of their similar free-fall timescale due to their nearly uniform density. It, therefore, induces a quick increase of the accretion rate, that allows the formation of the central protostar. The density profile quickly steepens at the center, the density at 10 AU increasing from less than 5×10^6 to 10^{10} cm^{-3} in 2×10^4 yr, and follows an asymptote with a power-law index of ~ 1.5. Since the temperature profile increases with the protostar luminosity and the protostar mass, the temperature in the protostellar envelope also quickly increases from less to 10 K to 200 K at 10 AU. After the formation of the central protostar, the accretion rate slowly decreases because of the slow and gradual collapse of each shell located outside R_f.

In spite of its relative simplicity, the physical model used in this work is in fair agreement with the observations of molecular clouds, dense cores, and Class 0 protostars regarding their timescales and their physical profiles, as shown in Table 1 and Figure 1. Table 1 compares the lifetimes derived from the observations with the timescales obtained with the physical model. It can be seen that all the timescales obtained with the model lie in the range of values deduced from the observations, derived as explained below.

By analysing the IRAS survey carried out by Beichman et al. (1986), Ward-Thompson et al. (1994) estimated a total lifetime of ~ 1 Myr for prestellar cores detected in the submillimeter continuum. The more recent c2d *Spitzer* legacy project has yielded shorter lifetimes. Enoch et al. (2008) and Evans et al. (2009) estimated the lifetime of prestellar cores to be ~ 0.45 Myr with variation from cloud to cloud between 0.23 Myr in the Serpens cloud and 0.78 Myr in Perseus. A significant fraction of cores displays internal motions of contractions. The analysis of the line profiles of ~ 200 sources by Lee et al. (1999) has shown that 3 % of them display contraction signatures. However, more recent studies by Gregersen & Evans (2000) and Lee et al. (2004b) show that about 10-20 % of them are contracting. Assuming a total prestellar core lifetime between 0.23 and 0.78 Myr gives a lifetime of static cores $t_{\rm SC}$ and contracting cores $t_{\rm CC}$ of $2 \times 10^5 - 7 \times 10^5$ and $2 \times 10^4 - 1.6 \times 10^5$ yr, respectively. By comparing the number of Young Stellar Objects in different stages detected in various clouds, Evans et al. (2009) and Maury et al. (2011) estimated the lifetime of Class 0 protostars $t_{\rm C0}$ of $1 - 1.6 \times 10^5$ yr and $0.4 - 1 \times 10^5$ yr, respectively.

Figure 1 compares the physical profiles obtained with our model with observations of dark cores and low-mass protostars. Red crosses represent the temperatures and velocities obtained towards L1498 by Lee et al. (2001), Ward-Thompson et al. (2002), and Tafalla et al. (2004)

from observations of CS, N_2H^+ and $C^{18}O$ transitions, from continuum observations obtained with *ISO* and from the modelling of the emission of NH_3 line transitions assuming a thermal coupling between dust and gas, respectively. As can be seen in Fig. 1, the temperature and velocity profiles obtained with our model are in fair agreement with the observations at the edge of the core.

Green plus symbols in Figure 1 stand for the density, temperature, and velocity values derived by Kristensen et al. (2012) and Mottram et al. (2013) for a sample of low-mass protostars observed by the *Herschel Space Observatory*. For each model, only the observed protostars whose envelope masses are lower than the mass of the modelled core are shown. The density profiles obtained with our model are in good agreement with the observational values at 1000 AU while they are slightly higher than the values observationally derived at the inner regions (< 50 AU) of the protostellar envelopes. The discrepancy probably results from the break of the 1D symmetry in the inner 100 AU and the eventual formation of protoplanetary disks during the Class 0 phase (see Pineda et al. 2012, for instance). The temperatures of the warm inner region reached at the end of the Class 0 phase lie in the range of the observed values while the predicted temperatures at the external part of the envelope seem to be slightly higher than the observations, probably induced by the coupling between the dust and gas temperatures assumed in our model. The velocity profiles in the external protostellar envelopes obtained with our model assuming a free-fall collapse lie in the range of the values derived observationally. However, the 1D free-fall collapse assumed in our model is not necessarily correct in the inner few hundreds of AU and would tend to overestimate the infall velocity occurring in the hot corino.

3.2. *Chemical differentiation of ices in dark clouds*

3.2.1. *Reference model*

The physical model used in this work allows us to follow the multilayer formation of interstellar ices from the sparse translucent phase of molecular clouds to the dense and cold phase seen at the center of dark cores. Figures 2, 3, 4, and 5 present the evolution of the physical and chemical properties of a shell located at the center of the model A-F as a function of the ice deposition profile. The time corresponding to any layer represents the time at which the layer has been formed.

Fig. 2 shows the evolution of the physical properties ($n_{\rm H}$, T, A_V) and time with the formation of ices. Most of the ice formation occurs in molecular clouds since about 80 % of the ice monolayers are formed when $n_{\rm H} < 5\times10^4$ cm^{-3} and $A_{V,\rm mod} < 10$ mag. Consequently, only 20 % of the ices has been formed in cold ($T < 10$ K) and dense ($n_{\rm H} > 5 \times 10^4$ cm^{-3}) conditions.

The evolution of the physical conditions induces an evolution of the gas phase chemistry shown in Fig. 3 for a selection of important gaseous species and for the main ice components. In particular, the abundances of atomic C, O, and N do not display the same evolution. Atomic C is quickly transferred to CO via reactions in the gas phase while the abundance of atomic O slowly decreases because of its freezes-out onto the grain surfaces forming icy species, or through reactions in the gas phase forming gaseous species such as O_2. The modelled abundance of O_2 is several orders of magnitude higher than the observations of molecular clouds carried out with space telescopes (see Larsson et al. 2007; Liseau et al. 2012). Atomic nitrogen shows a decrease of its abundance due to its freeze-out on the grains and through reactions in the gas phase. Since CO is the main destroyer of N_2H^+, its depletion in dense core conditions tends to re-increase the abundance of N-bearing species, such as N_2H^+, NH_3 or N, at the end of the calculation. This effect has already been observed by Bergin et al. (2001) and Tafalla et al. (2002) and previously modelled by Bergin & Langer (1997) and Aikawa et al. (2001). The gas phase abundances of the main icy components lie within a few orders of magnitude since some species (CH_3OH) are only formed at the surface of grains and are then evaporated through non-thermal processes while others (H_2O, H_2CO, NH_3) can also be formed in the gas phase and show higher abundances.

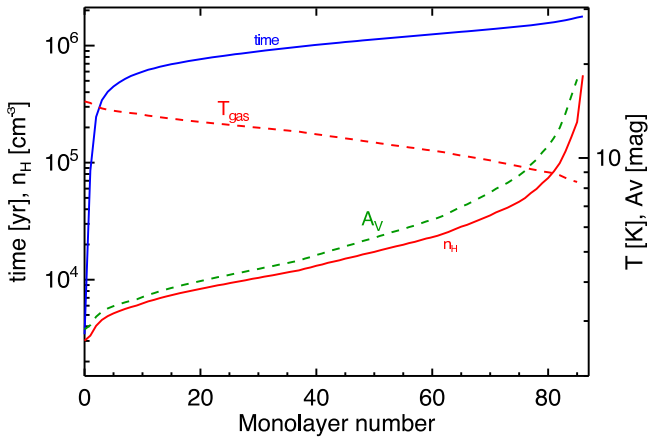

FIG. 2.— Evolution of the physical properties as function of the number of layers formed in the ices obtained for a shell at the center of model A-F.

The mantle of cold interstellar ices is believed to be mostly inert (Watanabe et al. 2004). The chemical composition of each layer would, therefore, reflect the physical and chemical properties at the moment of its formation. Figure 4 shows the chemical composition of each layer within interstellar ices formed with our reference model. It can be seen that the ices are very heterogeneous and their chemical structure depends on the evolution of both the physical properties and the gas phase abundances (see also Garrod & Pauly 2011; Taquet et al. 2013a; Vasyunin & Herbst 2013). Water and carbon dioxide are mostly formed in the inner parts of ices when the density is limited with high atomic abundances, and when the temperature is warm, allowing the diffusion of heavier species, such as CO, O, or OH, to recombine together to form CO_2. As the density increases and the temperature decreases with time, CO freezes-out onto the grains and is gradually destroyed to form H_2CO and CH_3OH instead of CO_2. Interestingly, NH_3 shows high abundances in the inner and outer parts of the ices. The high abundance in the inner part is due to the high abundances of H and N that favour the hydrogenation of atomic N on grains while the high abundance at the surface of the ice is due to the increase of N-bearing species in the gas phase at high CO depletions.

As mentioned in the introduction, the deuteration of

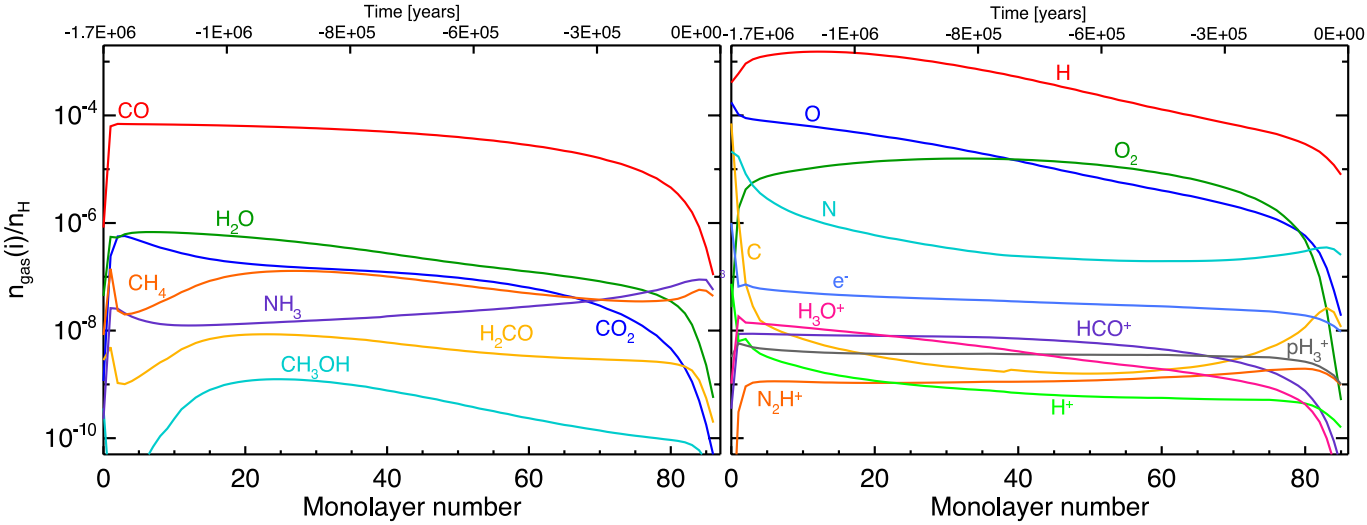

FIG. 3.— Evolution of the gas phase abundances of important species as function of the number of layers formed in the ices obtained for a shell at the center of model A-F.

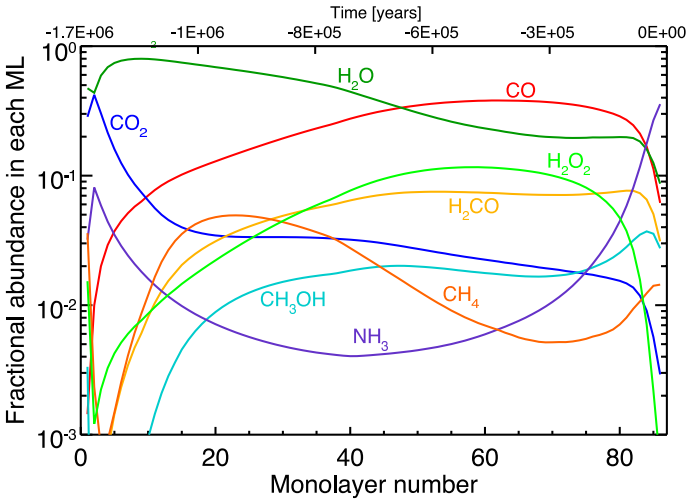

FIG. 4.— Fractional composition in each ice monolayer as function of the number of layers formed in the ices obtained for a shell at the center of model A-F.

gaseous and icy species depends on several physical (density, temperature) and chemical (opr(H_2), X_{gas}(CO)) parameters. Hydrogenated icy species are mostly formed through hydrogenation reactions triggered by the irradiation of H atoms at the surface of interstellar grains. The atomic [D]/[H] abundance ratio in the gas phase, therefore, governs the deuteration on the ices.

The effect of these two chemical parameters on the deuteration can be seen in Fig. 5 showing the evolution of the deuteration in the gas phase and in each ice monolayer, overplotted with the evolution of opr(H_2) and X_{gas}(CO), whose values are shown on the right axis, as function of the ice deposition profile. The timescale needed to decrease opr(H_2) and X_{gas}(CO) are similar to the timescale of the total ice formation. The two parameters slowly decrease during most of the ice formation, keeping high values ($> 10^{-3}$ and $> 10^{-5}$, respectively) up to 70-80 MLs, inducing a slight increase of the deuteration both in the gas phase and on ices. The decrease of these two crucial parameters is enhanced at the end of the ice formation for dense core conditions, and generates a sharp increase of the deuteration of doubly and even more triply deuterated species near the surface. It can be seen that the deuteration of water, ammonia, formaldehyde, and methanol in the gas phase reflects the deuteration within each monolayer which, in turn, roughly follows the evolution of the atomic D/H abundance ratio in the gas phase, reaching values higher than 10 % at the end of ice formation. Doubly deuterated species show fractionations higher than 1 % while triply deuterated forms of methanol show D/H ratios higher than 10^{-4} at the surface.

The deuteration of gaseous water seems to be slightly enhanced compared to the evolution of the atomic D/H ratio and the deuteration of formaldehyde and methanol. It is due to its efficient deuteration in the gas phase through ion-neutral reactions, as also predicted by the gas phase calculations of Roberts et al. (2004). CH_2DOH and CH_3OD show similar deuteration profiles but their final abundances in the outermost layers differ by ~ 60 %. The difference is due to the abstraction reactions occurring only on the methyl group of methanol introduced in our chemical network following the experiments by Hidaka et al. (2009).

3.2.2. *Influence of input parameters*

We have investigated the influence of several physical and chemical parameters on the formation and the deuteration of interstellar ices. For this purpose, we varied the values of the parameters listed in Table 4 to our reference model. Table 7 and Table 8 of the Appendix present the ice composition and the deuteration of water, formaldehyde, and methanol obtained when the density reaches the observed value for the considered core (L1498: $n_{\rm H,0,obs} = 2 \times 10^5$ cm^{-3} for model A and L1544: $n_{\rm H,0,obs} = 4 \times 10^6$ cm^{-3} for model B).

The variation of the five physical properties (type of core, initial density, initial external visual extinction, initial external temperature, and timescale for the static formation) slightly influence the chemical composition of ices, in particular the conversion from CO to CO_2 and to H_2CO and CH_3OH. CO_2 is mainly formed at the beginning of the molecular cloud phase, through reactions involving heavy particles, at low-density and warm conditions ($T > 12$ K) while H_2CO and CH_3OH are rather

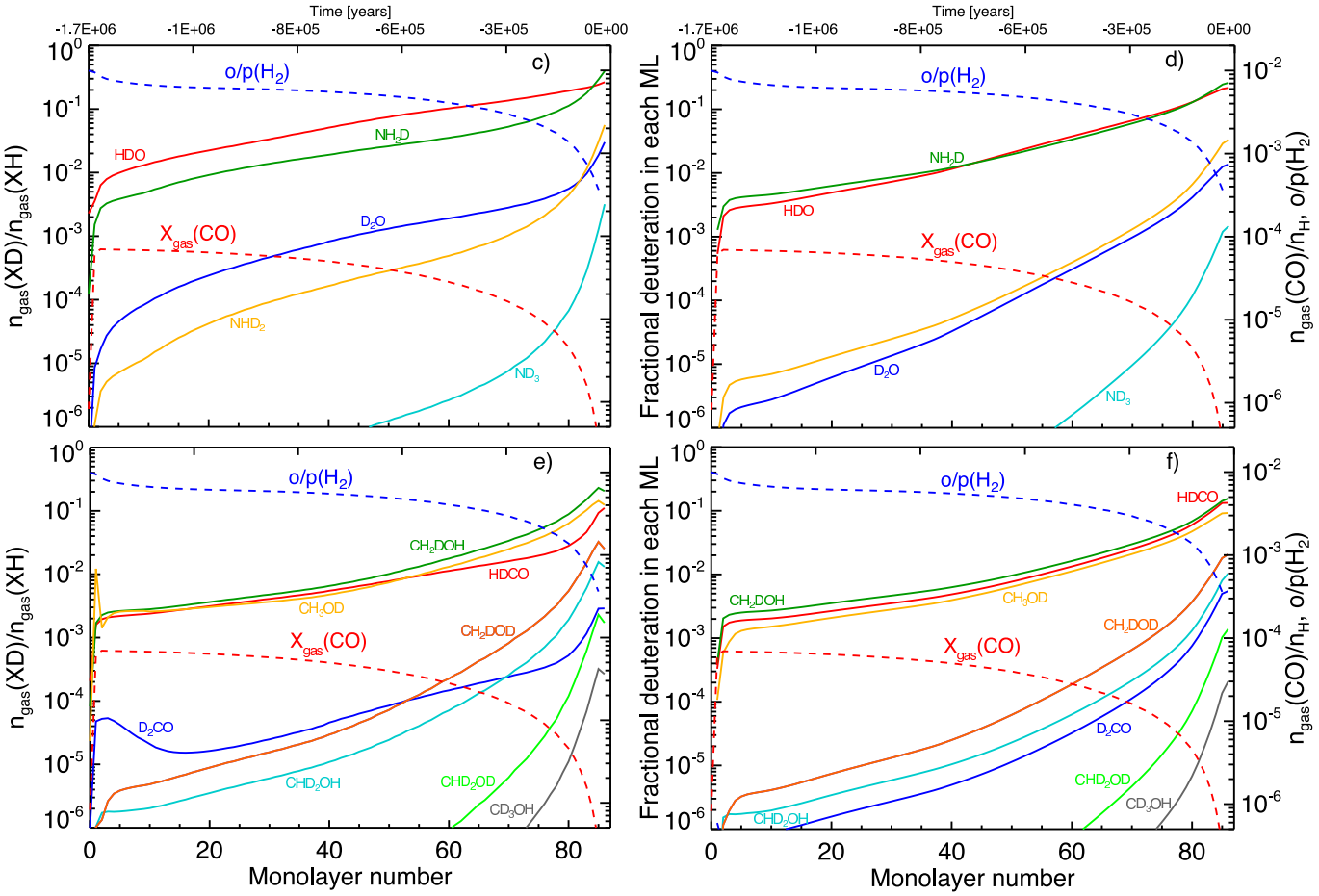

FIG. 5.— Evolution of the gas phase deuteration (left) and the icy deuteration in each layer (right) for water and ammonia (top) and for formaldehyde and methanol (bottom) as function of the number of layers formed in the ices obtained for a shell at the center of model A-F. The evolution of the gaseous CO abundance and the ortho/para ratio of H_2 are overplotted in dashed lines and their values are shown on the right axis.

formed in the external part of ices for dense and colder conditions. The increase of the initial density decreases the abundance of H atoms in the gas phase and, therefore, the efficiency of hydrogenation reactions forming formaldehyde and methanol in competition with the H_2O and CH_4 formation. The increase of the initial visual extinction decreases the photodesorption of reactive particles and, therefore, increases the efficiency of surface reactions. The increase of the temperature increases the mobility of heavy species allowing the formation of CO_2, but also the mobility of H atoms in dense core conditions when the H/CO abundance ratio is high, enhancing the formation of formaldehyde and methanol.

The surface parameters, namely the binding energies of light particles and the diffusion to desorption energy ratio, strongly influence the chemical composition of ices because the rates of surface reactions depend exponentially on them. Therefore, the increase of E_b and E_d/E_b strongly decrease the abundances of surface molecules formed through reactions with activation energies (CO_2, H_2CO, and CH_3OH). These two parameters are, therefore, the two most important parameters for the chemical composition of ices. By following the multilayer ice formation during a free-fall collapse with their Monte-Carlo model, Vasyunin & Herbst (2013) observed the same influence of the diffusion-to-binding energy ratio on the chemical composition of ices. The comparison of our modelling results with typical interstellar ice abundances deduced from infrared observations of ices show that, although the chemical composition of most species strongly depend on E_d/E_b and E_b, the reference models give predictions that are in fair agreement with observations. Overall, CO_2 tends to be slightly underproduced while H_2CO, CO, and NH_3 show overpredictions of their abundances.

Not surprisingly, the most important parameter for the deuterium chemistry is the initial value of the opr of H_2. Since the timescale needed to decrease the opr(H_2) is similar to the timescale of total ice formation, a high initial opr(H_2) value of 3 gives a final opr(H_2) of $\sim 5\times10^{-2}$ (see Fig. 6 showing the evolution of the opr of H_2, the CO abundance in the gas phase, and the atomic gaseous D/H abundance ratio as function of the normalized ice deposition profile for each model). The deuteration reactions are, therefore, strongly limited by the high abundance of o-H_2 throughout the formation of dense cores, decreasing the deuterium fractionation of reactive ions, such as the p-D_2H^+/o-H_2D^+ and N_2D^+/N_2H^+ abundance ratios, by more than one order of magnitude. Since the overall deuteration of icy species is governed by the atomic D/H abundance ratio in the gas phase which is, in turn, mostly governed by the deuteration of H_3^+ (Roberts et al. 2003; Taquet et al. 2012b), the deuteration in ices is also reduced by more than one order of magnitude.

The variation of other chemical and physical parameters has only a moderate impact on the atomic gaseous [D]/[H] abundance ratio and, therefore, on the ice deuteration since they do not influence the variation of opr(H_2) and X_{gas}(CO) as it can be seen in Fig. 6. The three parameters roughly follow the same trend for all the parameters explored in this work, except when the opr(H_2) is varied. The deuteration in ices is, therefore, almost independent of these parameters. The variation of the overall ice deuteration seen in Table 8 is mainly due to the variation of their moment of formation within ices. For instance, the increase of the initial temperature increases the abundance of methanol which is also located in the inner and less deuterated part of ices.

3.3. *Spatial evolution in dark cores*

The abundances and deuterations profiles of the main ice components in the gas phase and in ices, obtained when the density profile reaches the observed profile of L1498, are shown in Figures 7 and 8. Every species shows a decrease of the abundance in ices towards the edge of the core, mainly due to the high flux of UV photons which photo-evaporates and photo-dissociates interstellar ices. However, the abundances of formaldehyde and methanol decrease more strongly, by five orders of magnitude, and at lower radius ($r \sim 1.5 \times 10^4$ AU) than other species because of the warm temperature reached at the edge of the core that favours the CO_2 formation from CO instead of formaldehyde and methanol. Unlike interstellar ices, the abundances in the gas phase of most of icy species tend to increase towards the edge of the core because they are governed by the balance between their formation through the evaporation from grains supported by an eventual formation in the gas phase (for CO, H_2O, H_2CO, or NH_3) and their depletion through the freeze-out on grains in the center of cores or their photodissociation at the edge of the cores. Thus, the gas-phase abundances of most of species tend to deplete towards the center because of the increase of the density, enhancing the accretion rate, and the decrease of the temperature that decreases the evaporation rate. Species that are more strongly bound to the ices and that do not show any efficient formation in the gas phase, such as CO_2 and CH_3OH, display lower abundances at the center. In contrast, and as already discussed previously, NH_3 abundance tends to increase towards the center of the core because its formation in the gas phase and on ices is enhanced by the CO depletion.

As shown in Fig. 8, the icy and gaseous deuterations of all species increase towards the center of the core, because of the increase of the density and the decrease of the temperature which decrease X_{gas}(CO) and opr(H_2). The deuteration of all simply deuterated isotopologues is of a few percents in ices except for the deuteration of ammonia which is about 20 % because of its late formation. The deuteration of methanol decreases more strongly towards the edge of the core than for other species because CH_3OH deuteration is not efficient at warmer temperatures while gas phase reactions can still account for the deuteration of H_2O, H_2CO, and NH_3. The deuteration of all icy species in the gas phase is higher than the overall deuteration in ices by about one order of magnitude. This is due to the deuteration differentiation in ices; the deuteration of the gas phase roughly scales with the deuteration of the highly deuterated surface of ices while the overall deuteration in ices also includes the inner and poorly deuterated ice mantle.

3.4. *Ice evaporation in Class 0 envelopes*

Once the free-fall timescale of the core is reached, the protostar formation starts influencing the chemical abundance profiles through the warm-up of the protostellar envelope. Figure 9 presents the gas phase abundance profiles in the protostellar envelope of the collapsing core A-F for the main ice components obtained at the beginning and at the end of the Class 0 phase. As shown in section 3.1, the strong increase of the accretion rate induces a quick increase of the temperature in the protostellar envelope. The multilayer approach used to follow the evolution of interstellar ices induces complex abundance profiles with double abundance jumps for solid species that are more volatile than water (see also Vasyunin & Herbst 2013; Garrod 2013).

For species like CO, CO_2, CH_4, or H_2CO, the abundance profiles can be distinguished into three regimes:
i) the cold external envelope, where $T < T_{ev,i}$ (where $T_{ev,i}$ is the temperature of sublimation of species i), in which the abundance profile in the gas phase of each species i is governed by the balance between its formation from gas phase reactions and photo-evaporation and its destruction through the freeze-out on grains and its photodissociation. The decrease of the abundances towards the protostar is due to the increase of the density, as the accretion rate becomes more efficient, and to the increase of the visual extinction, decreasing the photodesorption rates.
ii) the cold intermediate envelope, where $T_{ev,i} < T < T_{ev,\mathrm{H2O}}$, in which a part of their icy content evaporates thermally when the temperature reaches their temperature of sublimation through the diffusion of volatile particles towards the surface. However, most of their volatile content stays trapped into the ices.
iii) the warm inner envelope, where $T > T_{ev,\mathrm{H2O}}$, in which all the icy material is evaporated with water in the gas phase when $T = T_{ev,\mathrm{H2O}} \sim 100 - 110$ K via the so-called "volcano desorption" (Collings et al. 2004).
The abundance profiles of species showing similar or higher binding energies than water do not display the second regime. Since the temperature in the protostellar envelope increases with the age of the protostar while the density decreases, the gas phase abundances tend to increase with time, inducing a disappearance of the double desorption peaks for some species, and an increase of the size of the hot corino region.

As it can be seen in Figure 10, the deuteration of all species but ammonia is higher in the external envelope than in the hot corino. The D/H ratio predicted in the hot corino reflects the overall deuteration of ices whereas the deuteration of the external envelope is due to the sublimation of the highly deuterated ice surface through non-thermal processes and eventually supported by a gas phase chemistry. At the beginning of the Class 0 phase, the D/H ratio of simply deuterated species is about 10 times higher in the cold envelope, at $r = 3000$ AU, than in the hot corino, at $r = 10$ AU. This is in good agreement with the difference of deuteration between icy and gaseous molecules predicted in dense cores. A peak of the deuteration is observed between 20 and 100 AU, cor-

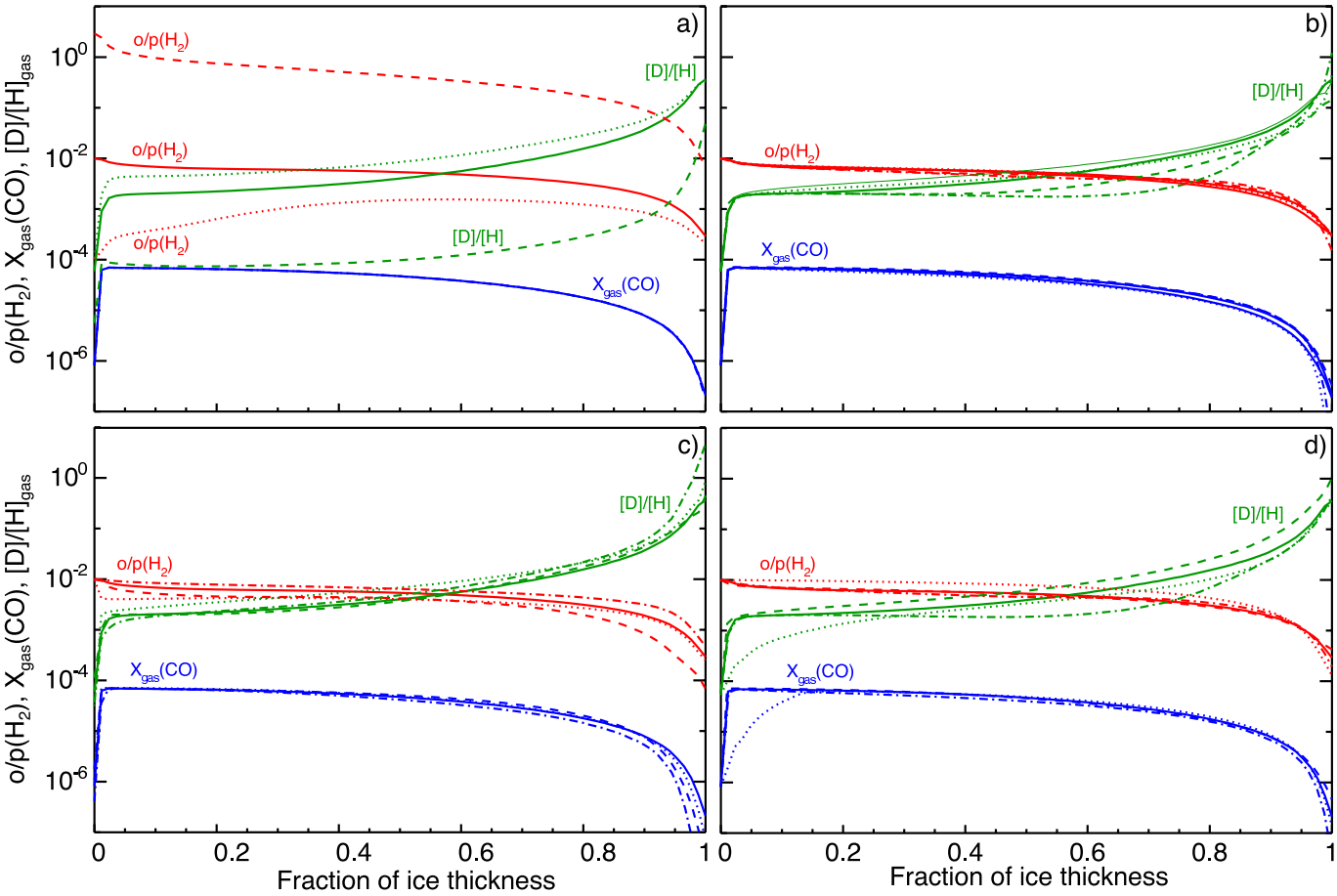

FIG. 6.— Evolution of H_2 opr, gas phase abundance of CO, and gaseous atomic [D]/[H] abundance ratio as a function of the normalized thickness of interstellar ices. a) Solid lines: reference model, dotted lines: opr(H_2) = 10^{-4}, dashed lines: opr(H_2) = 3. b) Solid lines: reference model, dotted lines: $E_d/E_b = 0.5$, dashed lines: $E_d/E_b = 0.8$, dotted-dashed lines: E_b(H) = 400 K, thin solid lines: E_b(H) = 600 K. c) Solid lines: reference model, dotted lines: $A_V = 1$ mag, dashed lines: $t_{\rm BC} = 2 \times t_{\rm BC,0}$, dotted-dashed lines: model B. d) Solid lines: reference model, dotted lines: $n_{\rm H,ini} = 10^4$ cm^{-3}, dashed lines: $T_{\rm d,ext} = 14$ K , dotted-dashed lines: $T_{\rm d,ext} = 20$ K.

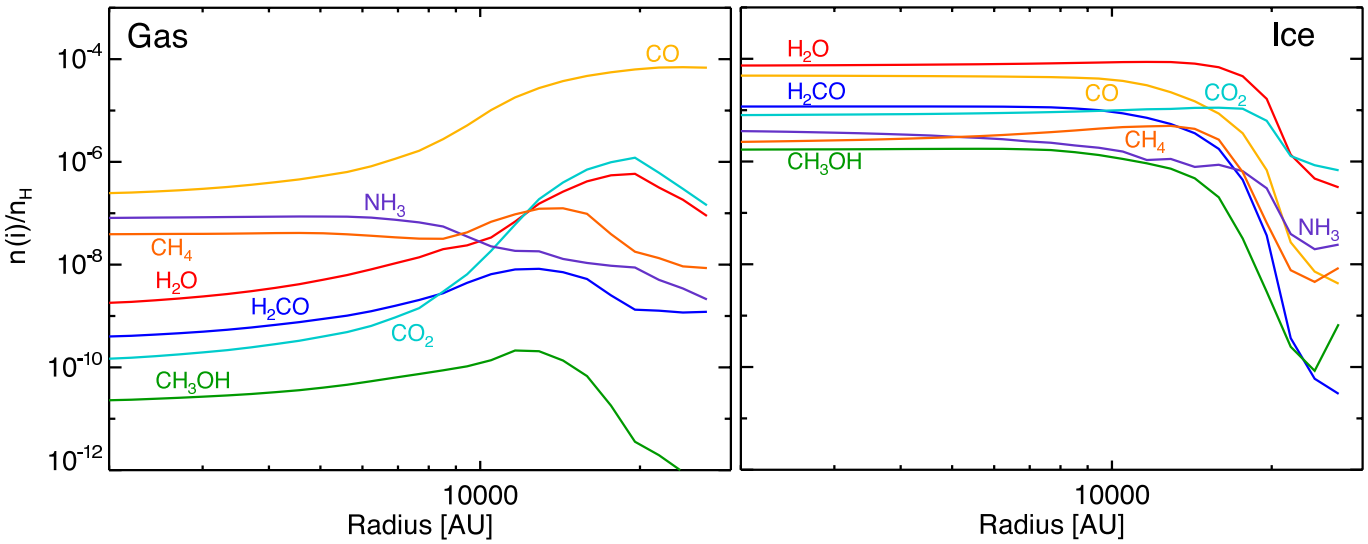

FIG. 7.— Abundance profiles in the gas phase (left) and in ices (right) of the main ice components obtained for the L1498 model obtained when the density profile reaches the observed profile.

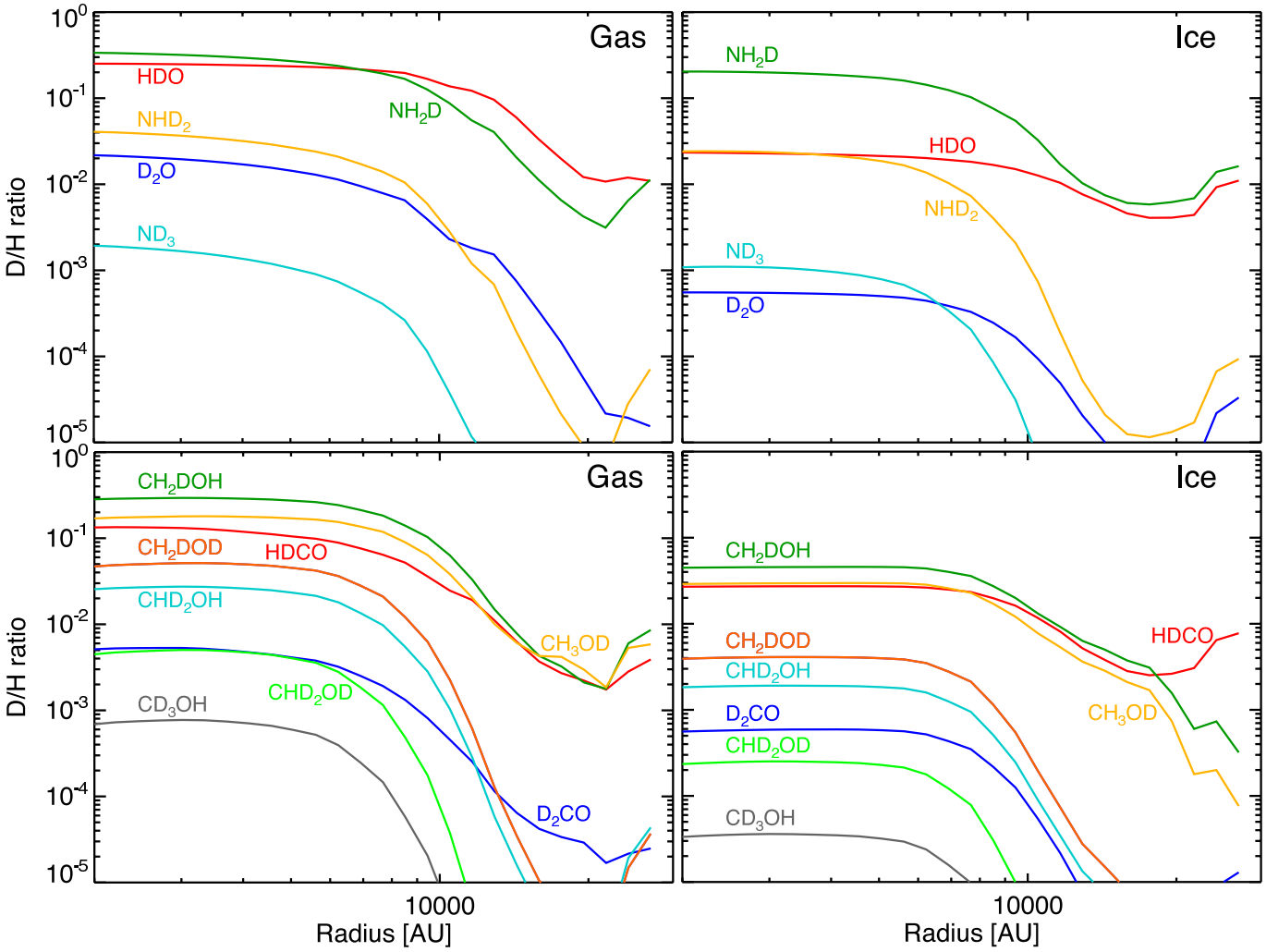

FIG. 8.— Deuteration profiles in the gas phase (left) and in ices (right) of the main ice components obtained for model A-F obtained when the density profile reaches the observed profile.

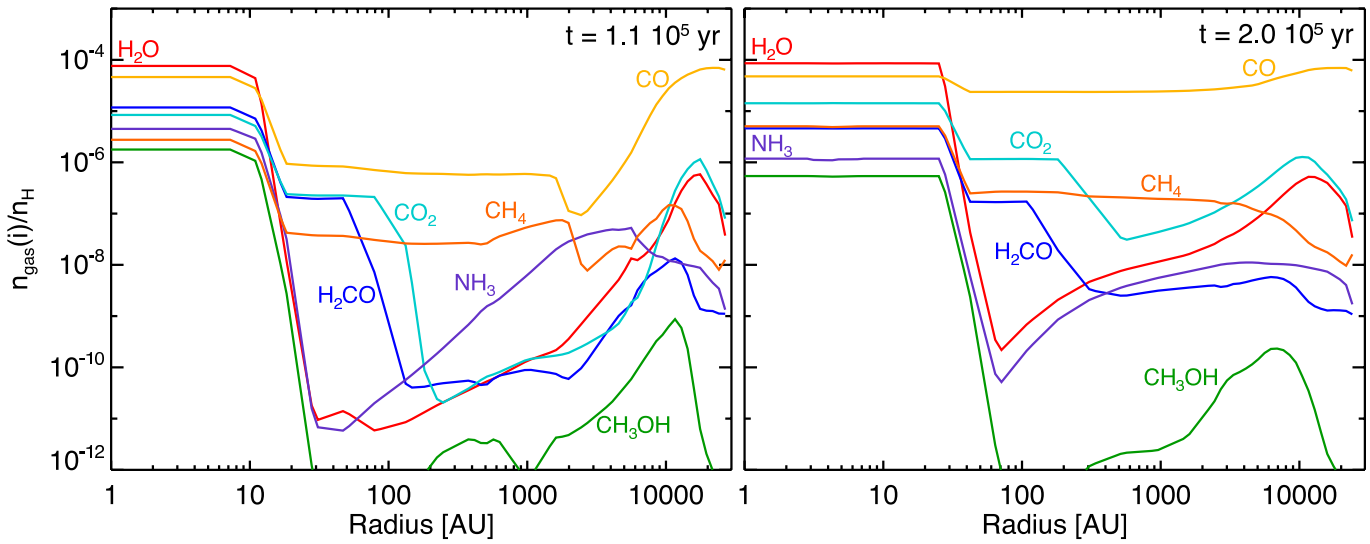

FIG. 9.— Gas phase abundance profiles of the main ice components obtained for the collapsing core A-F at the beginning (left) and at the end (right) of the Class 0 phase.

responding the zone where interstellar ices start to sublimate at $T \sim 100$ K during the fast collapse. Since deuterated species are mostly located at the surface, they mostly evaporate before their main isotopologue which are rather located in the inner part of the ice, increasing the D/H abundance ratio in the gas phase in the evaporation zone.

During the evolution of the Class 0 phase, the deuteration of simply and doubly deuterated species in the hot corino decrease by one and more than two orders of magnitude respectively, due to the gradual collapse of each shell of the envelope (see Table 6 for deuteration values of various species). At the beginning of the Class 0 phase, the gas seen in the hot corino ($1 < r < 30$ AU) comes from the shells located at $r \sim 5000$ AU whereas the warm gas modelled at the end of the Class 0 phase originates from shells located at $r \sim 1.5 \times 10^4$ AU where the deuteration is lower. Although the deuteration of water in the hot corino decreases with the age of the protostar, its deuteration remains roughly constant in the external envelope. This is due to gas phase reactions and in particular to the recombination reactions between highly deuterated OH radicals, and their deuterated isotopologues, in the gas phase at $50 < T < 100$ K that form highly deuterated water.

3.5. *Consequences on complex organics deuteration*

We modelled the formation and the deuteration of complex organics at the surface of interstellar grains through radical recombinations and hydrogenation reactions by incorporating the surface chemical network of Garrod et al. (2008). We only focused our study on a few prototype COMs; methyl formate ($HCOOCH_3$), methyl cyanide (CH_3CN), di-methyl ether (CH_3OCH_3), and formic acid (HCOOH) whose sub-millimetric spectra of their deuterated isotopologues have recently been measured in laboratories (Margulès et al. 2010; Cazzoli et a. 2011; Richard et al. 2013; Nguyen et al. 2013; Coudert et al. 2013), allowing recent and future detections towards low-mass protostars. Figure 11 presents the spatial distributions of the gas phase abundances of methanol and the four COMs in the protostellar envelope of the collapsing core A-F at the beginning and the end of the Class 0 phase.

In our model, methyl formate and di-methyl ether are mostly formed through radical recombination reactions ($HCO + CH_3O$ for methyl formate and $CH_3 + CH_3O$ for di-methyl ether) at the surface of warm interstellar grains ($30 < T < 50$ K), triggered by the photodissociation of the main ice constituents from the cosmic ray induced UV field. Formic acid is thought to be mostly formed in cold ices in dark clouds through the reaction sequence

$$CO + OH \rightarrow HO\text{-}CO\ (+H) \rightarrow HCOOH \qquad (8)$$

as suggested by laboratory and theoretical works (Goumans et al. 2008; Ioppolo et al. 2011). The reaction between HCO and OH also plays a minor role. Two main routes play a major role in the formation of methyl cyanide as it can be formed either in cold ices through the hydrogenation sequence of C_2N or during the warm-up phase through the radical recombination between CH_3 and CN.

Complex organics desorb thermally in the hot corino when the temperature reaches their temperature of sublimation. A part of the particles formed on ices also evaporates through non-thermal processes at lower temperature, generating the complex abundance profiles shown in Fig. 11. The abundances of methyl formate and dimethyl ether tend to increase with the age of the protostar because the timescale of the warm-up phase (when $30 < T < 50$ K) required for an efficient formation of COMs increases with the age of the protostar. Like water and carbon dioxide, the abundance of formic acid remains roughly constant with the evolutionary stage because it is efficiently formed throughout the precursor dark core, unlike methyl cyanide whose abundance decreases by one order of magnitude because of its lower formation at the edges of the core.

The deuteration of the simply deuterated isotopologues of COMs in the hot corino is shown in Table 6 along with the deuteration of the main ice components. It can be seen that the deuteration roughly scales with the deuteration of their parent molecules. Since methyl formate and di-methyl ether are mostly formed at the external surface of warm ices from the photodissociation of highly deuterated formaldehyde and methanol, their deuterium fractionation is high (up to ~ 20 %) at the beginning of the Class 0 phase and decreases with time. The fractionation of $HCOOCH_2D$ is larger than that of $DCOOCH_3$ because formaldehyde, forming HCO (and DCO) through photodissociation, is less deuterated than methanol, forming CH_3O (and its deuterated isotopologues) at the surface of ices. A significant part of formic acid and methyl cyanide is formed in the less deuterated phase of dark clouds, their D/H abundance ratio is consequently lower (1 - 2 % and 3.5 %, respectively). As for the main ice species, the deuteration of COMs decreases with the age of the protostar from one to two orders of magnitude.

4. DISCUSSION

4.1. *Comparison with previous models*

One of the goals of this work is the study of the spatial and temporal evolutions of the deuterium chemistry within protostellar envelopes. It is therefore worth comparing our results with those by Aikawa et al. (2012) although the two approaches differ slightly. Aikawa et al. (2012) adopted a more simple astrochemical model, assuming a homogeneous ice chemistry and neglecting the spin states of H_2 and other ions important for the deuterium chemistry but they adopted a more sophisticated hydrodynamical model than ours.

The most striking difference is found for the spatial evolution of abundances and deuterations within prestellar cores. Our model predicts stronger decreases of the abundances and deuterations of the main icy species towards the edge of the core than the model by Aikawa et al. (2012). These differences are likely due to the use of the multilayer approach in this work which makes the ice chemistry much more dependent on the physical parameters than the standard approach that assumes homogeneous ices (see Taquet et al. 2012a). The temporal evolution of the gaseous deuteration predicted at the center of protostellar envelopes is consequently much stronger in our work than in the work by Aikawa et al. (2012).

The comparison of our "early phase" results (at $t = 1.1 \times 10^5$ yr, see Table 6) with those by Aikawa et al.

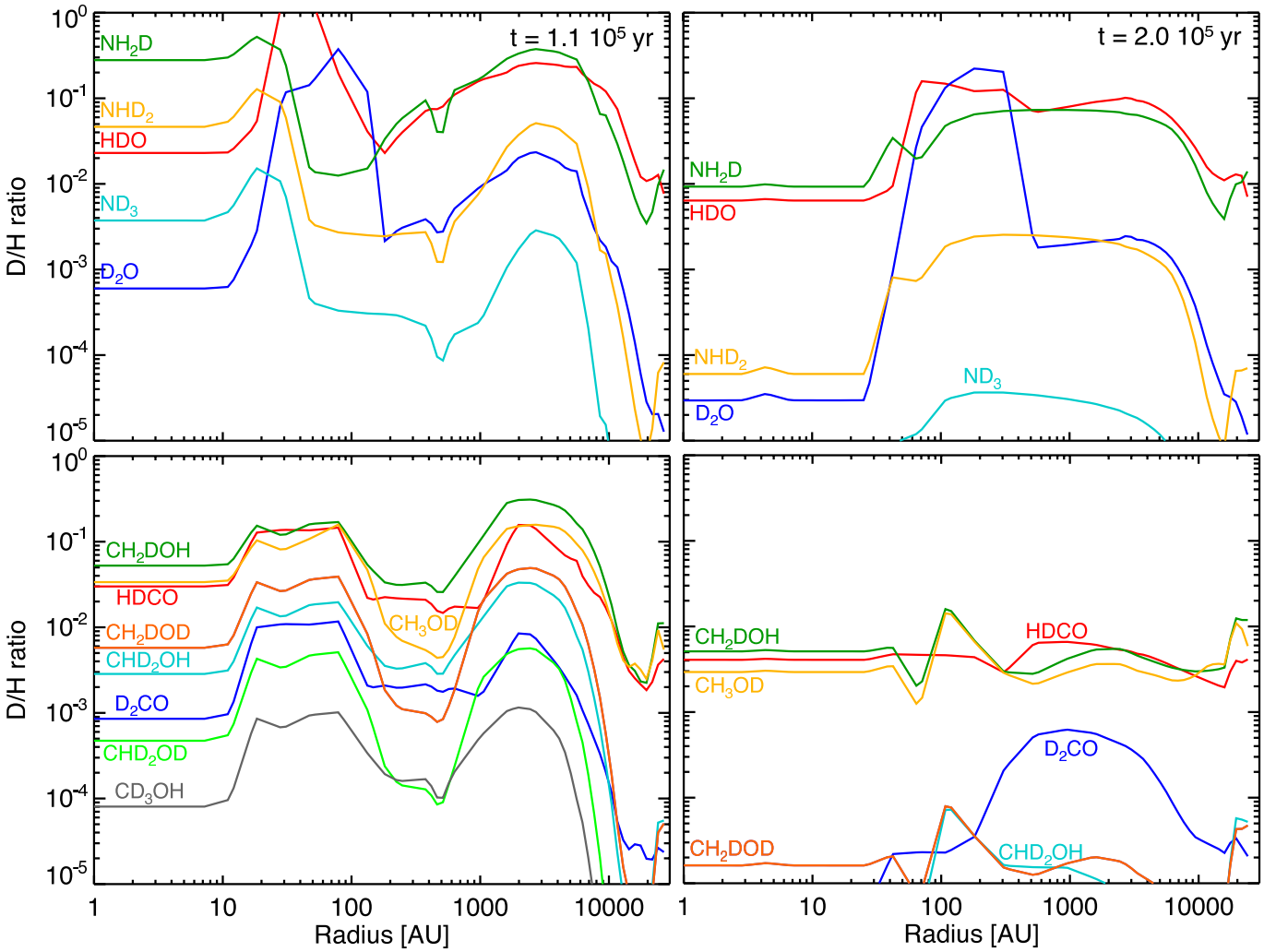

FIG. 10.— Gas phase deuteration profiles of the main ice components obtained for the collapsing core A-F at the beginning and at the end of the Class 0 phase.

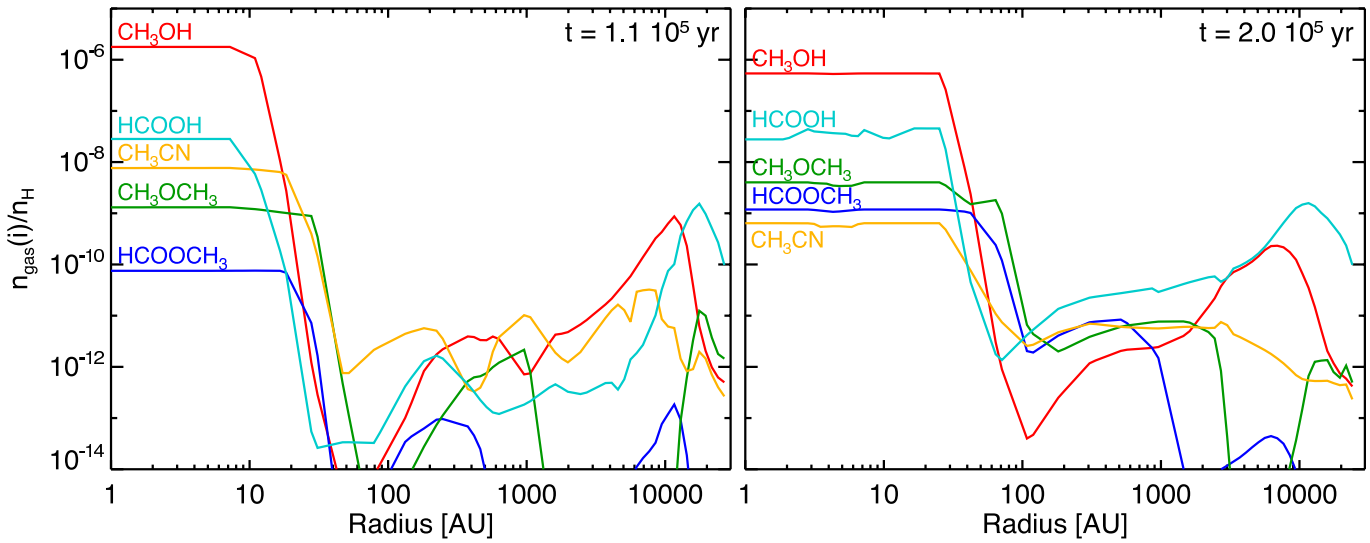

FIG. 11.— Gas phase abundance profiles of selected COMs thought to be mainly formed at the surface of interstellar grains obtained for the collapsing core A-F at the beginning and at the end of the Class 0 phase.

(2012) at $t = 9 \times 10^4$ yr shows that the two works predict a similar evolution of the water deuteration, with a D/H ratio of a few percents in the inner region and > 10 % in the cold external envelope. However, the deuteration of ammonia, formaldehyde, and methanol is 2 to 20 times higher in our work, because of their late formation at the surface of interstellar ices when the gas phase D/H ratio is high. We also note a discrepancy in the predictions of the deuteration of the COMs since we predicted higher deuteration for methyl formate than for formic acid and methyl cyanide (> 10 % versus $1 - 4$ %) while Aikawa et al. (2012) predicted a higher deuteration for methyl cyanide and formic acid (7 and 50 %) than for methyl formate (1 %).

4.2. *Comparison with observations*

4.3. *Abundances*

Table 7 of the Appendix compares the chemical composition of interstellar ices predicted by GRAINOBLE with infrared observations of ices towards dense cores. Observational data is taken from Öberg et al. (2011) who summarized results obtained by Boogert et al. (2011) towards a sample of dense cores and compared them with the *Spitzer* c2d Legacy ice survey carried out towards low-mass protostars. It can be seen that, even if surface parameters strongly influence the ice composition as discussed in section 3.2.2, the standard model seems to be in fair agreement with the ice observations, since the predicted abundance of most of species are close to the range of abundances given by the observations. However, the standard model tends to underpredict the formation of CO_2 (10 % versus 38 %) in favour of CO (65 % versus 31 %), and overestimates the H_2CO abundance compared to CH_3OH. An increase of the external temperature of 3 K ($T_{\rm ext} = 17$ to 20 K) significantly increases the abundance of CO_2 and CH_3OH, showing observable values. In all of the models, H_2CO is overproduced, implying that the destruction of H_2CO, forming CH_3OH, is not efficient enough. Laboratory studies have shown that H and D atoms can penetrate into a few surface layers (Watanabe et al. 2004; Ioppolo et al. 2010). The incorporation of such diffusion processes between several reactive surface layers in astrochemical models would, therefore, increase the efficiency of hydrogenation reactions and decrease the abundance of H_2CO in favour of CH_3OH.

Table 5 compares the predicted abundances of selected COMs with respect to that of methanol with the sub-millimetric observations towards a sample of low-mass protostars performed with single-dish telescopes. For a sake of consistency between all the molecules, all the observed values are derived from rotational diagram analysis, giving column densities averaged over the large beam of the single-dish telescope ($\theta_b = 10 - 30$ ″) that encompass the hot corino, and the cold external envelope. Absolute abundances are not presented since they strongly depend on the choice of the H_2 column density, which is quite uncertain. The predicted abundance ratios are, therefore, derived from column densities averaged over a beam of a radius $R_b = 3000$ AU (~ 30 ″ at 200 pc, the averaged distance of the observed low-mass protostars).

As for ices, our model strongly overpredicts the abundance of H_2CO in protostellar envelopes. We predict a gaseous H_2CO/CH_3OH abundance ratio of ~ 10 while the gaseous H_2CO/CH_3OH abundance ratio observed in the gas phase of protostellar envelopes is consistent with that observed in ices (~ 30 %), suggesting that the gas phase chemistry does not alter significantly their relative abundance after their evaporation. The comparison between predicted and observed abundances of COMs gives contrasting results. On the one hand, the abundance ratios of CH_3CN and HCOOH are in good agreement with observations. While the predicted CH_3CN abundance ratio tends to decrease with the age of the protostar, it remains within the range of observed values, which are roughly constant from source to source (between 0.5 and 1.9 %). The HCOOH abundance ratio predicted at the beginning of the Class 0 stage lie in the range of observed values while the late prediction slightly overestimates the ratio. On the other hand, the abundance of $HCOOCH_3$ and CH_3OCH_3, considered as late-stage molecules, is underpredicted by our model by one to three orders of magnitude, showing that the formation of these molecules is still not completely understood. The predicted abundances of these two COMs barely exceed 1 % with respect to methanol whereas observations show that their abundance should easily exceed 10 % in some cases. Because of the fast collapse considered in our one-dimension model, molecules that are evaporated at $T > 100$ K stay in the hot corino for ~ 100 yr before being accreted by the protostar. Warm gas phase chemistry is not efficient enough to produce complex organics in significant quantities (Horn et al. 2004). Experimental studies and molecular dynamics simulations have demonstrated that UV photons can penetrate into the inner part of interstellar ices, up to ~ 100 monolayers (Gerakines et al. 2001; Andersson et al. 2008), triggering a bulk chemistry induced by the mobility of photoproducts. Garrod (2013) introduced a three-phase approach in order to treat the bulk chemistry, allowing the formation of complex organics in the ice mantle. However, the predicted abundance ratios of $HCOOCH_3$ and CH_3OCH_3 do not exceed 1 % for the three types of physical models considered in his work, suggesting that bulk chemistry does not seem to be efficient enough to produce complex organics.

4.3.1. *Deuterium fractionations*

The deuterium fractionation of various species predicted by our model is compared with sub-millimetric observations of low-mass protostars in Table 6. As for Table 5, the predicted deuterations are derived from the beam-averaged column densities for two typical sizes. $R_b = 50$ AU corresponds to a small beam of 0.4 ″ obtained with sub-millimetric interferometers, such as PdBi, SMA, or ALMA, while $R_b = 3000$ AU corresponds to a large single-dish beam of 30 ″. As already mentioned in the introduction, the deuteration of water has been extensively studied in a sample of low-mass protostars with different telescopes (ground-based and space telescopes, single-dish and interferometers) and with different methods (standard LTE and non-LTE LVG models based on constant and spherical physical structures) giving contrasting results. By taking all the results together into account, the warm $[HDO]/[H_2O]$ ratio originating from the hot corino shows a large range of values, from 0.04 to 8 %, while the water deuteration of the cold envelope is about 0.3 - 18 % (see the discussion in Coutens et al.

TABLE 5
Modelled and observed abundances (in %) of COMs relative to CH_3OH in protostellar envelopes.

	Model (R_b = 3000 AU)		Observations				
	$t = 1.1 \times 10^5$ yr	$t = 2.0 \times 10^5$ yr	I16293	I2A	I4A	I4B	Ref.
H_2CO	870	1400	20 - 33	25 - 36	11 - 17	17 - 26	1, 2
$HCOOCH_3$	0.011	0.44	21 - 57	< 85	30 - 91	2.6 - 31	3, 4, 5
CH_3OCH_3	0.24	1.45	11 - 64	< 52	< 21	< 19	3, 4, 5
CH_3CN	1.7	0.59	0.50 - 1.50	0.68 - 1.6	0.9 - 1.8	0.98 - 1.9	3, 4, 5
HCOOH	6.2	38	5.2 -6.5	< 13	0 - 12	< 14	3, 4, 5

Note. — 1: van Dishoeck et al. (1995) for I16293 2: Maret et al. (2004) for I2A, I4A, I4B 3: Cazaux et al. (2003) for I16293 4: Bottinelli et al. (2004) for I4A 5: Bottinelli et al. (2007) for I2A and I4B

2013b) which are in good agreement with our predictions since the predicted HDO/H_2O and D_2O/H_2O abundance ratios decrease with the age of the protostar within the large range of values given by the observations. However, the more recent observations using sub-mm interferometers and the *Herschel Space Observatory* have refined the results. Interferometric observations, with high angular resolution allowing astronomers to probe the hot corino region of protostellar envelopes, have yielded low HDO/H_2O abundance ratios of $0.05 - 0.3$ % (Persson et al. 2013, 2014.) while *Herschel* observations, more sensitive to the external envelope, show that the cold water shows a higher deuteration of $\sim$ 1 % (Coutens et al. 2013b). This trend is confirmed by our astrochemical model. The deuteration in the hot corino scales with the overall deuteration of interstellar ices and includes the poorly deuterated inner mantle whereas the deuteration of the cold envelope, induced by the evaporation of highly deuterated ice surfaces and supported by the cold gas phase chemistry, remains roughly constant and shows higher values of a few %. The deuteration of water, therefore, increases with the size of the beam, by a factor 2 to 10, showing that the highly deuterated external and cold protostellar envelopes can contribute significantly to the overall deuteration observed with single-dish telescopes, in spite of their low abundance.

Formaldehyde and methanol show very high deuterium fractionations, with observed $HDCO/H_2CO$ and CH_2DOH/CH_3OH abundance ratios of $\sim$ 20 and $\sim$ 50 %, respectively. Such high fractionations are not reproduced by our model, since the highest D/H ratios of formaldehyde and methanol, reached at the beginning of the Class 0 phase, are $\sim$ 4 and $\sim$ 5.5 %, respectively, a factor of 4 and 9 lower than the observed values. For all the protostars observed by Parise et al. (2006), the rotational diagram analysis give lower rotational temperatures for deuterated formaldehyde and methanol isotopologues than for their main isotopologue, suggesting that deuterated species would originate from colder regions than their main isotopologue. As shown in Fig. 8, the high observed deuteration can indeed be reached in the external envelope, between r = 1000 and 5000 AU but the absolute abundances of deuterated formaldehyde and methanol in the external envelope are too low to increase the beam-averaged deuteration. The CH_3OD/CH_3OH abundance ratio predicted at the beginning of the Class 0 phase lies in the range of observational values. CH_3OD is thought to be formed only via addition reactions since abstraction reactions that enhance the deuteration of methanol seem to occur only on the methyl group of methanol. The abstraction reactions are, therefore, not efficient enough to increase the abundances of CH_2DOH, CHD_2OH, and CD_3OH. As shown in Fig. 4, methanol is present in a significant part of ices, and not only in the outermost layers, as it was predicted in the pseudo-time dependent calculations assuming constant physical conditions (Taquet et al. 2012b). While the multilayer approach considered here only considers one reactive surface, the diffusion of H and D atoms into the bulk would tend to increase the deuteration of methanol and the $[CH_2DOH]/[CH_3OD]$ abundance ratio since more CH_3OH molecules will be available to react. Other processes, such as H/D exchange between water and methanol, or gas phase reactions can also play an important role in the evolution of the $[CH_2DOH]/[CH_3OD]$ ratio (Charnley et al. 1997; Ratajczak et al. 2009).

The deuteration of methyl formate, methyl cyanide, and dimethyl ether, observed towards I-16293, are in fair agreement with our model predictions. They confirm that methyl formate and dimethyl ether, thought to be mainly formed from highly deuterated ices during the warm-up phase in protostellar envelopes, show higher deuterations than methyl cyanide which would also be formed in the cold anterior phase. This comparison tends to valid the formation mechanisms and the moment of formation of these three molecules. Now that sub-millimetric spectra have been measured and constrained by laboratory experiments for other COMs, the deuterium fractionation of COMs observed in protostellar envelopes can be used as a chemical tracer to understand their chemical history through the interpretation of their moment and their mechanisms of formation.

5. CONCLUSIONS

In this work, we have theoretically followed the chemical evolution of interstellar ices from the translucent phases of molecular clouds to the envelopes of low-mass protostars by focusing on their deuterium fractionation. For this purpose, we coupled a gas-grain astrochemical model, following the multilayer formation and the evaporation of ices, with a one-dimensional dynamical/radiative transfer model of collapsing core. The main conclusions of this work are summarized below.

1) Interstellar ices predicted by our model present a chemical heterogeneity, in agreement with infrared observations of ices. Water and carbon dioxide are mostly formed in the inner part of the ice mantle while carbon monoxide, formaldehyde, and methanol are closer to the ice surface. Ammonia is present in the innermost and outermost ice layers.

2) Interstellar ices display an evolution of the deuteration within the mantle, the deuteration of all species increasing towards the surface by several orders of magnitude. This is due to the slow formation of ices from

TABLE 6
Modelled and observed deuterium fractionations (in %) of selected species in protostellar envelopes and comets.

	Model				Low-mass protostars			Comets		
	$t = 1.1 \times 10^5$ yr		$t = 2.0 \times 10^5$ yr		D/H	Source	Ref.	D/H	Source	Ref.
	50 AU	3000 AU	50 AU	3000 AU						
HDO	2.3	4.5	0.65	2.2	In: 0.04 - 8	4 protostars	1 - 8	0.032 - 0.092	8 comets	22, 23
					Out: 0.3 - 18		3, 6, 9			
D_2O	0.062	0.11	0.0036	0.043	In: 0.007	IRAS 16293	3	/	/	/
					Out: 0.03		3			
HDS	4	3.8	0.54	0.65	5 - 15	IRAS 16293	10	< 40	Hale-Bopp	24
D_2S	0.28	0.28	0.00094	0.0021	0.6 - 1.8	IRAS 4A	11	/	/	/
NH_2D	29	31	0.99	4.3	7.0 - 10	2 protostars	10, 12	< 24	Hale-Bopp	24
NHD_2	5.1	3.8	0.0074	0.11	2.6 - 3.0	IRAS 16293	13	/	/	/
ND_3	0.44	0.21	0.000057	0.0012	0.09	NGC 1333	14	/	/	/
DCN	18	18	0.46	1.1	0.40 - 7.1	17 protostars	15, 16	0.2	Hale-Bopp	25
HDCO	4.1	3.8	0.42	0.43	2.2 - 170	7 protostars	15, 17	< 10	Hale-Bopp	24
D_2CO	0.18	0.16	0.00064	0.0092	4.6 - 44	7 protostars	17	/	/	/
CH_2DOH	5.5	5.6	0.51	0.51	37 - 65	4 protostars	17	< 3.2	Hale-Bopp	24
CH_3OD	3.5	3.5	0.3	0.3	1.6 - 4.7	4 protostars	17	< 12	Hale-Bopp	24
CHD_2OH	0.31	0.31	0.00078	0.00076	7.4 - 25	3 protostars	17	/	/	/
CD_3OH	0.0092	0.0092	0.0016	0.0016	0.20 - 1.4	IRAS 16293	18	/	/	/
$DCOOCH_3$	9.2	/	0.0025	/	15	IRAS 16293	19	/	/	/
$HCOOCH_2D$	21	/	0.65	/	/	/	/	/	/	/
CH_2DOCH_3	22	/	0.61	/	15	IRAS 16293	20	/	/	/
CH_2DCN	3.6	/	0.15	/	1.3	IRAS 16293	21	/	/	/
DCOOH	2.3	/	0.58	/	/	/	/	/	/	/
HCOOD	1	/	0.66	/	/	/	/	/	/	/

Note. — 1: Parise et al. (2005) 2: Coutens et al. (2012) 3: Coutens et al. (2013a) 4: Persson et al. (2013) 5: Visser et al. (2013) 6: Taquet et al. (2013b) 7: Persson et al. (2014.) 8: Coutens et al. (2013b) 9: Liu et al. (2011) 10: van Dishoeck et al. (1995) 11: Vastel et al. (2003) 12: Sakai et al. (2009) 13: Loinard et al. (2001) 14: van der Tak et al. (2002) 15: Roberts et al. (2002) 16: Jørgensen et al. (2004) 17: Parise et al. (2006) 18: Parise et al. (2004) 19: Demyk et al. (2010) 20: Richard et al. (2013) 21: C. Kahane (private communication), taken from the analysis of the TIMASSS survey Caux et al. (2011) 22: Weaver et al. (2008) 23: Hartogh et al. (2011) 24: Crovisier et al. (2004) 25: Meier et al. (1998)

the translucent phases of molecular clouds to the dense and cold phase of dense cores, and the slow decrease of two chemical parameters, the gas phase abundance of CO and the ortho/para ratio of H_2, that limit the deuterium chemistry,

3) The multilayer approach used to follow the formation and the evaporation of ices induces double abundance jumps of icy species more volatile than water in protostellar envelopes. A part of the volatile content stays trapped into the ices when the temperature exceeds the temperature of sublimation and is released when water ice evaporates at $T \sim 100$ K.

4) The deuteration of most hydrogenated species evolves within the envelopes of low-mass protostars. The deuteration predicted in the hot corino is generally lower than the deuteration of the external envelope. The difference of deuteration in the warm and cold envelopes is explained by the gradient of deuteration within interstellar ices. Only the external ice layers evaporate in the cold envelope through non-thermal processes while the inner part of ice mantles evaporates only in the hot corino.

5) The deuteration tends to decrease with the evolutionary stage of the protostar, due to the gradual collapse of the external shells of the protostellar envelope that are less deuterated because of their lower density.

6) We have modelled the deuteration of some complex organics (COMs) that are believed to be mainly formed at the surface of interstellar grains. The deuteration of COMs is very sensitive to their formation pathways and to their moment of formation, Consequently, the deuterium fractionation can be used as a tracer to interpret their chemical history.

7) The comparison with the observations gives contrasting results. The model successfully reproduces the evolution of the D/H abundance ratio of water within protostellar envelopes as recently observed with ground-based interferometers and the *Herschel Space Observatory*. It also reproduces the different D/H ratio of COMs recently observed with single-dish telescopes. However, it underestimates the very high deuteration of formaldehyde and methanol, suggesting that the understanding and the modelling of interstellar ices is still not well understood.

The kinetic data we used have been downloaded from the online database KIDA (Wakelam et al. 2012, http://kida.obs.u-bordeaux1.fr). This work was supported by NASA's Origins of Solar Systems and Exobiology Programs. V. T. acknowledges support from the NASA postdoctoral program. O.S. acknowledges support from the Academy of Finland grant 250741.

REFERENCES

Acharyya, K., Fuchs, G. W., Fraser, H. J., van Dishoeck, E. F. and Linnartz, H. 2007, A&A, 466, 1005-1012

Aikawa, Y., Ohashi, N., Inutsuka, S.-i., Herbst, E. and Takakuwa, S. 2001, ApJ, 552, 639-653

Aikawa, Y., Wakelam, V., Hersant, F., Garrod, R. T. and Herbst, E. 2012, ApJ, 760, 40

Albertsson, T., Semenov, D. A., Vasyunin, A. I., Henning, T. and Herbst, E. 2013, ApJS, 207, 27

Albertsson, T., Semenov, D. and Henning, T. 2014, ApJ, 784, 39
Avgul, N. N. and Kiselev, A. V. 1970, Chem. Phys. Carbon, 6, 1
Andersson, S., van Dishoeck, E. F. 2008, A&A, 491, 907-916
Beichman, C. A., Myers, P. C., Emerson, J. P., Harris, S., Mathieu, R., Benson, P. J. and Jennings, R. E. 1986 ApJ, 307, 337-349
Bergin, E. A. and Langer, W. D. 1997, ApJ, 486, 316
Bergin, E. A., Ciardi, D. R., Lada, C. J., Alves, J. and Lada, E. A. 2001, ApJ, 557, 209-225
Bergman, p. and Parise, B. and Liseau, R. and Larsson, B. 2011, A&A, 527, 39
Bisschop, S. E., Fraser, H. J., Öberg, K. I., van Dishoeck, E. F. and Schlemmer, S. 2006, A&A, 449, 1297-1309
Boogert, A. C. A., Huard, T. L., Cook, A. M., Chiar, J. E. et al. 2011, ApJ, 729, 92
Bottinelli, S., Ceccarelli, C., Lefloch, B. et al. 2004, ApJ, 615, 354-358
Bottinelli, S., Ceccarelli, C., Williams, J. P. and Lefloch, B. 2007, A&A, 463, 601-610
Caux, E., Kahane, C., Castets, A., Coutens, A., Ceccarelli, C. et al. 2011, A&A, 532, A23
Cazaux, S., Tielens, A. G. G. M., Ceccarelli, C., Castets, A., Wakelam, V., Caux, E., Parise, B. and Teyssier, D. 2003, ApJ, 593, L51-L55
Cazaux, S., Caselli, P. and Spaans, M. 2011, ApJ, 741, L34
Cazzoli, G., Puzzarini, C., Stopkowicz, S. and Gauss, J. 2011, ApJS, 196, 10
Ceccarelli, C., Caselli, P., Bockelée-Morvan, D., Mousis, O., Pizzarello, S., Robert, F. and Semenov, D. 2014, PPVI
Charnley, S. B., Tielens, A. G. G. M. and Rodgers, S. D. 1997, ApJ, 482, L203
Charnley, S. B. and Rodgers, S. B. 2009, Astronomical Society of the Pacific Conference Series, 420, 29
Coudert, L. H., Drouin, B. J., Tercero, B., Cernicharo, J., Guillemin, J.-C., Motiyenko, R. A. and Margulès, L. 2013, ApJ, 779, 119
Coutens, A., Vastel, C., Caux, E., Ceccarelli, C., Bottinelli, S., Wiesenfeld, L., Faure, A., Scribano, Y. and Kahane, C. 2012, A&A, 539, A132
Coutens, A., Vastel, C., Cazaux, S., et al. 2013, A&A, 53, A75
Coutens, A., Vastel, C., Cabrit, S., et al. 2013, A&A, 560, A39
Collings, M. P., Anderson, M. A., Chen, R., Dever, J. W., Viti, S., Williams, D. A. and McCoustra, M. R. S. 2004, MNRAS, 354, 1133-1140
Congiu, E., Fedoseev, G., Ioppolo, S., Dulieu, F., Chaabouni, H., Baouche, S., Lemaire, J. L., Laffon, C., Parent, P., Lamberts, T., Cuppen, H. M. and Linnartz, H. 2012, ApJ, 750, L12
Crapsi, A., Caselli, P., Walmsley, M. C. and Tafalla, M. 2007, A&A, 470, 221-230
Crovisier, J., Bockelée-Morvan, D., Colom, P., Biver, N., Despois, D., Lis, D. C. et al. 2004, A&A, 418, 1141-1157
Cuppen, H. M., Herbst, E. 2007, ApJ, 668, 294
Demyk, K., Bottinelli, S., Caux, E., Vastel, C., Ceccarelli, C., Kahane, C. and Castets, A. 2010, A&A, 517, A17
Dislaire, V., Hily-Blant, P., Faure, A., Maret, S., Bacmann, A. and Pineau Des Forêts, G. 2012, A&A, 537, A20
Enoch, M. L., Evans, II, N. J., Sargent, A. I., Glenn, J., Rosolowsky, E. and Myers, P. 2008, ApJ, 684, 1240-1259
Evans, II, N. J., Rawlings, J. M. C., Shirley, Y. L. and Mundy, L. G. 2001, ApJ, 557, 193-208
Evans, II, N. J., Dunham, M. M., Jørgensen, J. K., Enoch, M. L., Merín, B., van Dishoeck, E. F., Alcalá, J. M., Myers, P. C., Stapelfeldt, K. R., Huard, T. L., Allen, L. E., Harvey, P. M., van Kempen, T., Blake, G. A., Koerner, D. W., Mundy, L. G., Padgett, D. L. and Sargent, A. I. 2009, ApJS, 181, 321-350
Fayolle, E. C., Bertin, M., Romanzin, C., Michaut, X., Öberg, K. I., Linnartz, H. and Fillion, J.-H. 2011, ApJ, 739, L36
Fayolle, E. C., Bertin, M., Romanzin, C., Poderoso, H. A. M., Philippe, L., Michaut, X., Jeseck, P., Linnartz, H., Öberg, K. I. and Fillion, J.-H. 2013, A&A, 556, A122
Flower, D. R., Pineau Des Forêts, G., Walmsley, C. M. 2006, A&A, 449, 621-629
Fraser, H. J., Collings, M. P., McCoustra, M. R. S. and Williams, D. A. 2001, MNRAS, 327, 1165-1172
Furuya, K., Aikawa, Y., Nomura, H., Hersant, F. and Wakelam, V. 2013, ApJ, 779, 11
Galli, D., Walmsley, M. and Gonçalves, J. 2002, A&A, 394, 275-284
Garrod, R. T., Wakelam, V. and Herbst, E. 2007, A&A, 467, 1103-1115
Garrod, R. T., Weaver, S. L. W. and Herbst, E. 2008, ApJ, 682, 283-302
Garrod, R. T. and Pauly, T. 2011, ApJ, 735, 15
Garrod, R. T. 2013, ApJ, 765, 60
Gerakines, P. A., Moore, M. H. and Hudson, R. L. 2001, J. Geophys. Res., 106, 33381-33386
Goumans, T. P. M., Uppal, M. A. and Brown, W. A. 2008, MNRAS, 384, 1158-1164
Gregersen, E. M. and Evans, II, N. J. 2000, ApJ, 538, 260-267
Hartmann, L., Ballesteros-Paredes, J. and Bergin, E. A. 2001 ApJ, 562, 852-868
Hartogh, P., Lis, D. C., Bockelée-Morvan, D., de Val-Borro, M., Biver, N. et al. 2011, Nature, 478, 218-220
Hasegawa, T. I., Herbst, E. and Leung C. M. 1992, ApJ, 82, 167
Hasegawa, T. I. and Herbst, E. 1993, MNRAS, 261, 83-102
Hasegawa, T. I. and Herbst, E. 1993, MNRAS, 263, 589-606
Hidaka, H., Watanabe, M., Kouchi, A. and Watanabe, N. 2009, ApJ, 702, 291-300
Herrero, V. J., Galvez, O., Maté, B. and Escribano, R. 2010, Phys. Chem. Chem. Phys., 12, 3164-3170
Horn, A., Møllendal, H., Sekiguchi, O., Uggerud, E., Roberts, H., Herbst, E., Viggiano, A. A. and Fridgen, T. D. 2004, ApJ, 611, 605-614
Hornekær, L., Baurichter, A., Petrunin, V. V. and Luntz, A. C., Kay, B. D. and Al-Halabi, A. 2005, J. Chem. Phys., 122, 12
Hosokawa, T. and Omukai, K. 2009, ApJ, 691, 823-846
Hugo, E., Asvany, O. and Schlemmer, S. 2009, J. of Chem. Phys., 130, 164302
Ioppolo, S. and Cuppen, H. M. and Romanzin, C. and van Dishoeck, E. F. and Linnartz, H. 2010, Physical Chemistry Chemical Physics (Incorporating Faraday Transactions), 12, 12065
Ioppolo, S., van Boheemen, Y., Cuppen, H. M., van Dishoeck, E. F. and Linnartz, H. 2011, MNRAS, 413, 2281-2287
Loinard, L., Castets, A., Ceccarelli, C. et al. 2001, ApJ, 552, L163-L166
Ivezic, Z. and Elitzur, M. 1997, MNRAS, 287, 799-811
Jørgensen, J. K., Schöier, F. L. and van Dishoeck, E. F. 2004, A&A, 416, 603-622
Katz, N., Furman, I., Biham, O., Pirronello, V. and Vidali, G. 1999, ApJ, 522, 305-312
Keto, E. and Caselli, P. 2010, MNRAS, 402, 1625-1634
Kristensen, L. E., van Dishoeck, E. F., Bergin, E. A., Visser, R., Yıldız, U. A., San Jose-Garcia, I. et al. 2012, A&A, 2012, 542, A8
Kroes, G. J. and Andersson, S. 2005, IAU Symposium, 231, 427-442
Larsson, B., Liseau, R., Pagani, L., Bergman, P. et al. 2007, A&A, 466, 999-1003
Lattelais, M., Bertin, M., Mokrane, H., Romanzin, C., Michaut, X., Jeseck, P., Fillion, J.-H., Chaabouni, H. et al. 2011, A&A, 532, A12
Lee, C. W., Myers, P. C. and Tafalla, M. 1999, ApJ, 526, 788-805
Lee, C. W., Myers, P. C. and Tafalla, M. 2001, ApJS, 136, 703-734
Lee, C. W., Myers, P. C. and Plume, R. 2004, ApJS, 153, 523-543
Lee, J-E., Bergin, E. A. and Evans, N. J. 2004, ApJ, 617, 360-383
Le Gal, R., Hily-Blant, P., Faure, A., Pineau des Forêts, G., Rist, C. and Maret, S. 2013, in press
Linsky, J. L. 2003, Space Science Reviews, 106, 49-60
Liseau, R., Goldsmith, P. F., Larsson, B., Pagani, L. et al. 2012, A&A, 541, A73
Liu, F.-C., Parise, B., Kristensen, L., Visser, R., van Dishoeck, E. F. and Güsten, R. 2011, A&A, 527, A19
Loinard, L., Castets, A., Ceccarelli, C. et al. 2001, ApJ, 552, L163-L166
Maret, S., Ceccarelli, C., Caux, E. et al. 2004, A&A, 416, 577-594
Margulès, L., Huet, T. R., Demaison, J., Carvajal, M., Kleiner, I., Møllendal, H., Tercero, B., Marcelino, N. and Cernicharo, J. 2010, ApJ, 714, 1120-1132
Maury, A. J., André, P., Men'shchikov, A., Könyves, V. and Bontemps, S. 2011, A&A, 535, A77
Mouschovias, T. C., Tassis, K. and Kunz, M. W. 2006, ApJ, 646, 1043-1049

Meier, R., Owen, T. C., Jewitt, D. C., Matthews, H. E., Senay, M., Biver, N., Bockelee-Morvan, D. Crovisier, J. and Gautier, D. 1998, Science, 279, 1707
Mottram, J. C., van Dishoeck, E. F., Schmalzl, M., Kristensen, L. E., Visser, R., Hogerheijde, M. R. and Bruderer, S. 2013, A&A, 558, A126
Mumma, M. J. and Charnley, S. B. 2011, ARA&A, 49, 471-524
Noble, J. A., Congiu, E., Dulieu, F. and Fraser, H. J. MNRAS, 2012, 421, 768-779
Noble, J. A., Theule, P., Mispelaer, F., Duvernay, F., Danger, G., Congiu, E. and Dulieu, F. and Chiavassa, T. 2012, A&A, 543, A5
Öberg, K. I., Garrod, R. T., van Dishoeck, E. F. and Linnartz, H. 2009, A&A, 504, 891-913
Öberg, K. I., Boogert, A. C. A., Pontoppidan, K. M., van den Broek, S., van Dishoeck, E. F., Bottinelli, S., Blake, G. A. and Evans, II, N. J. 2011, ApJ, 740, 109
Oka, T. 2004, J. Mol. Spectr., 228, 635
Ossenkopf, V. and Henning, T. 1994, A&A, 291, 943-959
Nguyen, L., Walters, A., Margulès, L., Motiyenko, R. A., Guillemin, J.-C., Kahane, C. and Ceccarelli, C. 2013, A&A, 553, A84
Pagani, L., Vastel, C., Hugo, E., Kokoouline, V., Greene, C. H., Bacmann, A., Bayet, E., Ceccarelli, C., Peng, R. and Schlemmer, S. 2009, A&A, 494, 623-636
Pagani, L., Roueff, E. and Lesaffre, P. 2011, A&A, 739, L35
Parise, B., Ceccarelli, C., Tielens, A. G. G. M. et al. 2002, A&A, 393, L49-L53
Parise, B. and Castets, A. and Herbst, E. and Caux, E. and Ceccarelli, C. and Mukhopadhyay, I. and Tielens, A. G. G. M. 2004, A&A, 416, 159-163
Parise, B., Caux, E., Castets, A., Ceccarelli, C., Loinard, L., Tielens, A. G. G. M. et al. 2005, A&A, 431, 547-554
Parise, B., Ceccarelli, C., Tielens, A. G. G. M., Castets, A., Caux, E., Lefloch, B. and Maret, S. 2006, A&A, 453, 949-958
Ratajczak, A., Quirico, E., Faure, A., Schmitt, B. and Ceccarelli, C. 2009, A&A, 496, L21-L24
Persson, M. V., Jørgensen, J. K. and van Dishoeck, E. 2013, A&A, 549, L3
Persson, M. V., Jørgensen, J. K., van Dishoeck, E. and Harsono, D. 2014, ApJ, in press.
Pineda, J. E., Maury, A. J., Fuller, G. A., Testi, L., García-Appadoo, D., Peck, A. B., Villard, E. et al. 2012, A&A, 544, L7
Pizzarello, S. and Huang, Y. 2005, Geochim. Cosmochim. Acta, 69, 599-605
Ratajczak, A., Taquet, V., Kahane, C., Ceccarelli, C., Faure, A. and Quirico, E. 2011, A&A, 528, L13
Richard, C., Margulès, L., Caux, E., Kahane, C., Ceccarelli, C., Guillemin, J.-C., Motiyenko, R. A., Vastel, C. and Groner, P. 2013, A&A, 552, A117
Roberts, H. and Millar, T. J. 2000, A&A, 361, 388-398
Roberts, H., Fuller, G. A., Millar, T. J., Hatchell, J. and Buckle, J. V. 2002, A&A, 381, 1026-1038
Roberts, H., Herbst, E. and Millar, T. J. 2003, ApJ, 591, L41-L44
Roberts, H., Herbst, E. and Millar, T. J. 2004, A&A, 424,905-917
Rodgers, S. D. and Millar, T. J. 1996, MNRAS, 280, 1046-1054
Roueff, E., Lis, D. C., van der Tak, F. F. S., Gerin, M. and Goldsmith, P. F. 2005, A&A, 438, 585-598
Sakai, N., Sakai, T., Hirota, T. and Yamamoto, S. 2009, ApJ, 702, 1025-1035
Sandford, S. A. and Allamandola, L. J. 1990, ApJ, 355, 357-372
Sandford, S. A. and Allamandola, L. J. 1993, ApJ, 417, 815-825
Sipilä, O. 2012, A&A, 543, A38
Sipilä, O., Caselli, P. and Harju, J. 2013, A&A, 554, A92
Tafalla, M., Myers, P. C., Caselli, P., Walmsley, C. M. and Comito, C. 2002, ApJ, 569, 815-835
Tafalla, M., Myers, P. C., Caselli, P. and Walmsley, C. M. 2004, A&A, 416, 191-212
Taquet, V., Ceccarelli, C. and Kahane, C. 2012, A&A, 538, A42
Taquet, V., Ceccarelli, C. and Kahane, C. 2012, ApJ, 748, L3
Taquet, V., Peters, P. , Kahane, C., Ceccarelli, C., López-Sepulcre, A., Toubin, C., Duflot, D., Faure, A. and Wiesenfeld, L. 2013, A&A, 550, A127
Taquet, V., López-Sepulcre, A., Ceccarelli, C., Neri, R., Kahane, C., Coutens, A., Vastel, C. 2013, ApJ, 768, L29
Thi, W.-F., Woitke, P. and Kamp, I. 2010, MNRAS, 407, 232-246
Tielens, A. G. G. M. and Allamandola, L. J. 1987, Interstellar Processes, eds. D. J. Hollenbach, & H. A. Thronson, 134, 397-469
van der Tak, F. F. S., van Dishoeck, E. F., Evans, II, N. J. and Blake, G. A. 2000, ApJ, 537, 283-303
van der Tak, F. F. S., Schilke, P., Müller, H. S. P., Lis, D. C., Phillips, T. G., Gerin, M. and Roueff, E. 2002, A&A, 388, L53-L56
van Dishoeck, E. F., Blake, G. A., Jansen, D. J., and Groesbeck, T. D. 1995, ApJ, 447, 760
Vastel, C., Phillips, T. G., Ceccarelli, C. and Pearson, J. 2003, ApJ, 593, L97-L100
Vasyunin, A. I., Herbst, E. 2013, ApJ, 762, 86
Vidali, G., Ihm, G., Kim, H. and Cole, M. 1991, Surface Science Reports, 12, 4, 135-181
Visser, R., Jørgensen, J. K., Kristensen, L. E., van Dishoeck, E. F. and Bergin, E. A. 2013, ApJ, 769, 19
Wakelam, V. and Herbst, E. 2008, ApJ, 680, 371-383
Wakelam, V., Herbst, E., Loison, J.-C., Smith, I. W. M. et al. 2012, ApJS, 199, 21
Walmsley, C. M., Flower, D. R. and Pineau des Forêts, G. 2004, A&A, 418, 1035-1043
Ward-Thompson, D., Scott, P. F., Hills, R. E. and André, P. 1994, MNRAS, 268, 276-290
Ward-Thompson, D., André, P. and Kirk, J. M. 2002, MNRAS, 329, 257-276
Watanabe, N., Nagaoka, A., Shiraki, T. and Kouchi, A. 2004, ApJ, 616, 638-642
Watanabe, N., Kimura, Y., Kouchi, A., Chigai, T., Hama, T. and Pirronello, V. 2010, ApJ, 714, L233-L237
Weaver, H. A., A'Hearn, M. F., Arpigny, C., Combi, M. R., Feldman, P. D., Tozzi, G.-P., Dello Russo, N. and Festou, M. C. 2008, LPI Contributions, 1405, 8216
Whittet, D. C. B., Bode, M. F., Longmore, A. J. et al. 1988, MNRAS, 233, 321-336
Whitworth, A. P. and Ward-Thompson, D. 2001, ApJ, 547, 317-322

APPENDIX

TABLE 7
OBSERVED AND PREDICTED ABUNDANCES (IN %) OF SOLID SPECIES WITH RESPECT TO WATER ICE AT THE END OF THE PRESTELLAR CORE STAGE.

Model	H_2O	CO_2	CO	H_2CO + HCOOH	CH_3OH	NH_3	CH_4
A	100	10.5	64.8	16.3	2.4	6.0	3.0
B	100	10.9	93.9	16.3	1.8	12.0	1.5
A, $n_{\rm H,ini} = 3 \times 10^3$ cm^{-3}	100	10.5	64.8	16.3	2.4	6.0	3.0
A, $n_{\rm H,ini} = 1 \times 10^4$ cm^{-3}	100	7.7	56.7	13.1	1.9	13.2	6.7
A-F, $A_{\rm V,ext} = 1$ mag	100	8.6	74.9	12.5	1.3	5.2	1.0
A-F, $A_{\rm V,ext} = 2$ mag	100	10.5	64.8	16.3	2.4	6.0	3.0
A, $T_{\rm ext} = 14$ K	100	7.5	81.7	11.3	1.0	6.0	0.5
A, $T_{\rm ext} = 17$ K	100	10.5	64.8	16.3	2.4	6.0	3.0
A, $T_{\rm ext} = 20$ K	100	26.2	33.7	19.6	10.9	6.0	7.9
A, $t_{\rm BC} = 1.7 \times 10^6$ yr	100	10.5	64.8	16.3	2.4	6.0	3.0
A, $t_{\rm BC} = 3.4 \times 10^6$ yr	100	8.7	45.9	13.3	2.3	10.0	5.9
A-F, $E_d/E_b = 0.5$	100	14.9	5.4	7.8	20.8	4.5	20.0
A-F, $E_d/E_b = 0.65$	100	10.5	64.8	16.3	2.4	6.0	3.0
A-F, $E_d/E_b = 0.8$	100	9.6	93.3	1.4	0.0	6.3	0.4
A-F, $E_b = 400$ K	100	12.1	37.4	19.7	12.1	4.4	6.6
A-F, $E_b = 500$ K	100	10.5	64.8	16.3	2.4	6.0	3.0
A-F, $E_b = 600$ K	100	34.3	73.7	13.3	1.5	8.4	0.8
A-F, o/p$(H_2)_{\rm ini} = 10^{-4}$	100	10.5	64.7	16.2	2.4	6.0	3.0
A-F, o/p$(H_2)_{\rm ini} = 10^{-2}$	100	10.5	64.8	16.3	2.4	6.0	3.0
A-F, o/p$(H_2)_{\rm ini} = 3$	100	10.5	64.9	16.4	2.4	5.8	3.0
Observations	100	38^{41}_{32}	31	$2.8^{3.3}_{2.4}$	8^{10}_{7}	5^{6}_{4}	5^{7}_{4}

TABLE 8
Observed and predicted deuterations in the gas phase and in ices at the end of the prestellar core stage.

			Gas phase deuteration					
Model	p-D_2H^+/o-H_2D^+	N_2D^+	HDO	D_2O	HDCO	D_2CO	CH_2DOH	CHD_2OH
A	1.60(-01)	7.76(-01)	2.40(-01)	1.80(-02)	1.02(-01)	3.32(-03)	2.30(-01)	1.60(-02)
B	1.73(-01)	1.75(+00)	2.58(-01)	4.57(-02)	1.11(-01)	1.28(-03)	9.00(-02)	2.56(-03)
A, $n_{\rm H,ini} = 3 \times 10^3$ cm^{-3}	1.60(-01)	7.76(-01)	2.40(-01)	1.80(-02)	1.02(-01)	3.32(-03)	2.30(-01)	1.60(-02)
A, $n_{\rm H,ini} = 1 \times 10^4$ cm^{-3}	2.78(-01)	1.28(+00)	2.46(-01)	1.97(-02)	9.51(-02)	4.09(-03)	3.00(-01)	3.01(-02)
A-F, $A_{\rm V,ext} = 1$ mag	1.42(-01)	6.86(-01)	2.37(-01)	1.71(-02)	9.58(-02)	2.84(-03)	2.03(-01)	1.22(-02)
A-F, $A_{\rm V,ext} = 2$ mag	1.60(-01)	7.76(-01)	2.40(-01)	1.80(-02)	1.02(-01)	3.32(-03)	2.30(-01)	1.60(-02)
A, $T_{\rm ext} = 14$ K	1.16(-01)	6.98(-01)	2.15(-01)	1.61(-02)	4.00(-02)	9.60(-04)	7.38(-02)	1.44(-03)
A, $T_{\rm ext} = 17$ K	1.60(-01)	7.76(-01)	2.40(-01)	1.80(-02)	1.02(-01)	3.32(-03)	2.30(-01)	1.60(-02)
A, $T_{\rm ext} = 20$ K	2.27(-01)	7.47(-01)	2.49(-01)	1.70(-02)	1.74(-01)	8.54(-03)	3.49(-01)	4.12(-02)
A, $t_{\rm BC} = 1.7 \times 10^6$ yr	1.60(-01)	7.76(-01)	2.40(-01)	1.80(-02)	1.02(-01)	3.32(-03)	2.30(-01)	1.60(-02)
A, $t_{\rm BC} = 3.4 \times 10^6$ yr	3.11(-01)	1.18(+00)	2.33(-01)	1.09(-02)	8.65(-02)	3.84(-03)	3.43(-01)	3.93(-02)
A-F, $E_d/E_b = 0.5$	1.13(-01)	2.94(-01)	2.17(-01)	8.63(-03)	1.14(-01)	7.87(-03)	5.36(-01)	1.33(-01)
A-F, $E_d/E_b = 0.65$	1.60(-01)	7.76(-01)	2.40(-01)	1.80(-02)	1.02(-01)	3.32(-03)	2.30(-01)	1.60(-02)
A-F, $E_d/E_b = 0.8$	1.81(-01)	1.10(+00)	2.33(-01)	1.88(-02)	1.86(-02)	8.31(-04)	4.64(-02)	5.24(-04)
A-F, $E_b = 400$ K	2.01(-01)	8.89(-01)	2.43(-01)	1.45(-02)	1.32(-01)	5.06(-03)	2.68(-01)	2.30(-02)
A-F, $E_b = 500$ K	1.60(-01)	7.76(-01)	2.40(-01)	1.80(-02)	1.02(-01)	3.32(-03)	2.30(-01)	1.60(-02)
A-F, $E_b = 600$ K	1.19(-01)	4.56(-01)	2.20(-01)	1.49(-02)	9.11(-02)	3.53(-03)	2.69(-01)	2.11(-02)
A-F, o/p$(H_2)_{\rm ini} = 10^{-4}$	1.67(-01)	7.09(-01)	2.38(-01)	1.76(-02)	9.70(-02)	3.08(-03)	2.30(-01)	1.62(-02)
A-F, o/p$(H_2)_{\rm ini} = 10^{-2}$	1.60(-01)	7.76(-01)	2.40(-01)	1.80(-02)	1.02(-01)	3.32(-03)	2.30(-01)	1.60(-02)
A-F, o/p$(H_2)_{\rm ini} = 3$	1.54(-02)	4.24(-02)	1.06(-01)	6.89(-04)	1.29(-02)	6.41(-04)	9.09(-03)	2.43(-05)
Observations L1498	/	4.00(+00)						
Observations L1544	< 0.80	2.30(-01)			3.20(-01)	4.00(-02)		
			Ice deuteration					
			HDO	D_2O	HDCO	D_2CO	CH_2DOH	CHD_2OH
A			2.41(-02)	5.24(-04)	2.54(-02)	4.26(-04)	3.92(-02)	1.23(-03)
B			2.14(-02)	2.59(-04)	1.57(-02)	9.59(-05)	2.29(-02)	1.55(-02)
A, $n_{\rm H,ini} = 3 \times 10^3$ cm^{-3}			2.41(-02)	5.24(-04)	2.54(-02)	4.26(-04)	3.92(-02)	1.23(-03)
A, $n_{\rm H,ini} = 1 \times 10^4$ cm^{-3}			2.10(-02)	5.96(-04)	2.83(-02)	7.20(-04)	6.07(-02)	3.19(-03)
A-F, $A_{\rm V,ext} = 1$ mag			2.69(-02)	5.17(-04)	3.41(-02)	5.00(-04)	6.12(-02)	1.80(-03)
A-F, $A_{\rm V,ext} = 2$ mag			2.41(-02)	5.24(-04)	2.54(-02)	4.26(-04)	3.92(-02)	1.23(-03)
A, $T_{\rm ext} = 14$ K			2.47(-02)	2.75(-04)	2.20(-02)	1.24(-04)	3.42(-02)	3.70(-04)
A, $T_{\rm ext} = 17$ K			2.41(-02)	5.24(-04)	2.54(-02)	4.26(-04)	3.92(-02)	1.23(-03)
A, $T_{\rm ext} = 20$ K			2.36(-02)	6.91(-04)	1.78(-02)	5.31(-04)	1.42(-02)	6.52(-04)
A, $t_{\rm BC} = 1.7 \times 10^6$ yr			2.41(-02)	5.24(-04)	2.54(-02)	4.26(-04)	3.92(-02)	1.23(-03)
A, $t_{\rm BC} = 3.4 \times 10^6$ yr			2.32(-02)	6.62(-04)	3.35(-02)	7.60(-04)	6.01(-02)	2.69(-03)
A-F, $E_d/E_b = 0.5$			1.98(-02)	1.53(-04)	1.46(-02)	2.48(-04)	3.15(-02)	2.12(-03)
A-F, $E_d/E_b = 0.65$			2.41(-02)	5.24(-04)	2.54(-02)	4.26(-04)	3.92(-02)	1.23(-03)
A-F, $E_d/E_b = 0.8$			1.45(-02)	9.67(-05)	7.38(-03)	2.02(-05)	6.78(-03)	3.33(-05)
A-F, $E_b = 400$ K			1.97(-02)	5.10(-04)	1.53(-02)	3.76(-04)	1.04(-02)	3.52(-04)
A-F, $E_b = 500$ K			2.41(-02)	5.24(-04)	2.54(-02)	4.26(-04)	3.92(-02)	1.23(-03)
A-F, $E_b = 600$ K			2.86(-02)	6.16(-04)	3.59(-02)	7.04(-04)	6.38(-02)	2.37(-03)
A-F, o/p$(H_2)_{\rm ini} = 10^{-4}$			3.62(-02)	9.32(-04)	3.86(-02)	6.86(-04)	5.62(-02)	1.89(-03)
A-F, o/p$(H_2)_{\rm ini} = 10^{-2}$			2.41(-02)	5.24(-04)	2.54(-02)	4.26(-04)	3.92(-02)	1.23(-03)
A-F, o/p$(H_2)_{\rm ini} = 3$			1.33(-03)	1.59(-06)	6.35(-04)	5.43(-07)	1.06(-03)	1.35(-06)